A human-inspired framework for bipedal robotic walking design

Ryan W. Sinnet*, Shu Jiang and Aaron D. Ames

Department of Mechanical Engineering,
Texas A&M University,
College Station, TX 77843-3123, USA
E-mail: rsinnet@tamu.edu
E-mail: shujiang@tamu.edu
E-mail: aames@tamu.edu
*Corresponding author

Abstract: This work seeks virtual constraints, or *outputs*, that are intrinsic to human walking and utilises these outputs to construct controllers which produce human-like bipedal robotic walking. Beginning with experimental human walking data, *human outputs* are sought, i.e., functions of the kinematics of the human over time, which provides a low-dimensional representation of human walking. It will be shown that, for these outputs, humans act like linear mass-spring-dampers; this yields a time representation of the human outputs through *canonical walking functions*. Combining these formulations leads to *human-inspired controllers* that, when utilised in an optimisation problem, provably result in robotic walking that is as 'human-like' as possible. This human-inspired approach is applied to multiple human output combinations, from which it is determined which output combination results in the most human-like walking for a robotic model with mean human parameters.

Keywords: bipedal robotic walking; human walking; non-linear control; hybrid systems.

Reference to this paper should be made as follows: Sinnet, R.W., Jiang, S. and Ames, A.D. (2014) 'A human-inspired framework for bipedal robotic walking design', *Int. J. Biomechatronics and Biomedical Robotics*, Vol. 3, No. 1, pp.20–41.

Biographical notes: Ryan W. Sinnet received his BS in Electrical Engineering from the California Institute of Technology and MS in Mechanical Engineering from Texas A&M University. He is currently pursuing his PhD in Mechanical Engineering at Texas A&M University as a Graduate Research Fellow of the National Science Foundation. His research interests include robotic walking, hybrid systems, and prosthetics.

Shu Jiang earned her BS in Electrical Engineering from Hefei University of Technology and MS in Control Theory and Technology from Shanghai Jiao Tong University. She is currently pursuing her PhD in Mechanical Engineering at Texas A&M University. Her area of interest is human-like robotic walking.

Aaron D. Ames is an Assistant Professor in Mechanical Engineering at Texas A&M University with a joint appointment in Electrical and Computer Engineering. He received his BS in Mechanical Engineering and BA in Mathematics from the University of St. Thomas and MA in Mathematics and PhD in Electrical Engineering and Computer Sciences from the University of California, Berkeley. His research focuses on hybrid systems with a special emphasis on bipedal robots and Zeno behaviour. His work is supported by NSF grants CNS-0953823, CNS-1136104 and NHARP award 00512-0184-2009.

1 Introduction

The goal of this paper is to analyse human walking in the context of the human-inspired control framework developed in Ames (2011b) in an attempt to better understand the fundamental mechanisms underlying human walking and then to apply this understanding to the control of bipedal robots. Human walking has been studied extensively from the perspective of biomechanics under the auspices of several different schools of thought: researchers have studied forces and dynamics (Seireg and Arvikar, 1975; Winter, 1990) at the hip (Bergmann et al., 1993; Heller et al., 2001) and at the foot (Au et al., 2006; Rodgers, 1988). Force measurements and estimations are typically done with force plates and force loading-models (Scott and Winter, 1993). The estimated forces are then used with either inverse-dynamic models (Glitsch and Baumann, 1997; Siegler and Liu, 1997) or forward-dynamic models (Anderson and Pandy, 2001; Neptune et al., 2001; Pandy

and Berme, 1988). Researchers have also studied nervous system interaction (Bojanic et al., 2011; Cifrek et al., 2009).

The results mentioned give valuable insights into the underlying dynamics of human walking yet fail to provide a natural way of controlling bipedal robots. Doing so would require modelling the complex nervous and muscular system of a human; having such a complicated model would make it difficult to glean any insight and, moreover, would render such a system incapable of real-time implementation. In order to design a practical robotic controller which draws insight directly from human walking, one need only look to the method of human-inspired control which provides a heuristic and computationally-tractable method for obtaining human-like robotic walking gaits from measured human kinematics data. And this is precisely the focus of this paper.

1.1 Methodology

In order to overcome the difficulties associated with modelling human walking in all its complexity, human-inspired control chooses to look at the human walking system as a 'black box', focusing solely on the relationship between inputs and outputs. The general idea is to try to find the inputs necessary to produce a certain combination of outputs. It will be seen that the procedure proposed in this paper does this with ease and without the element of human discretion for the purposes of controller design. This concept of removing human judgement results in a less qualitative design process and mitigates the potential for human error. In this paper, outputs on the kinematics of human walking are presented which are purported to faithfully represent the human-walking gait. These outputs represent half of the 'black box'. The standard method of feedback linearisation will provide the other half, specifying a manner for determining the inputs which will produce the desired outputs.

This paper will codify the intuitive methodology presented above by defining a rigorous step-by-step process which can be applied to bipedal walking on flat ground. The process begins by considering experimental data representing the kinematics of human test subjects walking on flat ground at a 'natural' pace. The experimental results are used in a three-step process:

Step 1 Seek outputs that characterise human walking: *human outputs*, as computed from the kinematics of a human over the course of a step. Since these outputs are computed directly from experimental data, they consist of discrete sets of points.

Step 2 Represent the discrete output data using a class of time-dependent functions of the simplest yet most general form possible: *canonical walking functions*, representing the human output data as time-dependent functions.

Step 3 Given a bipedal robot, compute the outputs from the kinematics of the robot. A non-linear controller can be constructed, termed a *human-inspired controller*, which drives the output of a robot to the outputs of the human (as represented by the canonical walking functions). The parameters of the human-inspired controller are determined through a *human-inspired optimisation* that produces the best fit of the canonical walking functions to the human output data while simultaneously guaranteeing bipedal robotic walking.

By following the steps in this procedure, one will be able to obtain 'human-like' robotic walking which will be remarkably similar to the human walking from which it derives its inspiration.

Step 1 in the proposed approach to achieving human-like robotic walking is to determine outputs which appear to characterise human walking and which simultaneously are feasible for the purposes of robotic controller design. More specifically, for a given output to be usable, the following assumptions or *output criteria* (OC) must hold:

- (OC1) it is a function of the joint angles, i.e., it can be represented as a forward kinematics map
- (OC2) it has a 'simple' time-dependent representation; the simplicity will serve to illuminate the underlying structure of human walking
- (OC3) it is mutually exclusive from the other chosen outputs; the decoupling matrix associated with feedback linearisation is full rank on (and nearby to) the designed gait trajectory.

On first inspection, the above criteria provide a large number of possible output functions; in this paper, there are 12 specific outputs which are considered – these outputs and the motivation for choosing them are given in Section 2.3. From these 12 outputs, six combinations are chosen for study. The outputs are first categorised into four distinct sets on the basis of functionality – e.g., the angle of the stance knee naturally belongs to the set of functions whose members, in some qualitative capacity, represent the behaviour of the stance knee. By choosing one element from each of these four distinct sets, one should theoretically be able to obtain human-like walking for a robot; and, in fact, this paper does so for the six output combinations under investigation, providing results from various simulations. The six output combinations can be subdivided into two groups: three of the output functions use the hip position to parameterise time and, indeed, some work has been done in this respect (Sinnet et al., 2011); the other three outputs use the position of the centre-of-mass (CoM) as a parameterisation and, when combined with the accompanying outputs, yield a simple 'compass-gait' model which has been studied in depth (Ames et al., 2007; Espiau and Goswami, 1994; Goswami et al., 1998).

Prior work (Srinivasan et al., 2008, 2009; Joshi and Anand, 2010) has considered tracking joint angles to achieve robotic walking – while the joint angles of a human would satisfy criteria (OC1) and (OC3), they would not

necessarily satisfy criterion (OC2) – but this paper takes a more generalised approach, analysing functions of these joint angles. This more heuristic approach allows for a deeper understanding of the basic structures intrinsic to human walking.

Step 2 looks to discover a time-dependent representation of the human output functions in a manner which leads to insights into human walking. In particular, since the human outputs are discrete data points and cannot be applied to controller construction directly, one must represent the human outputs as time-dependent functions. The first contribution of this paper is the discovery that all the human outputs are accurately described (with a correlation coefficient of essentially one) by a very simple class of functions:

1 either a linear function of time

2 or the time solution to a linear mass-spring-damper system.

The simplicity and universality of these functions lend to the name *canonical walking functions*. Unlike other time-based functions that have been used to fit the human data in past work [polynomials (Kramer, 2010) and Bézier series in Westervelt et al. (2003)], the form of the canonical human walking functions provides insight into the underlying kinematics of human walking. One is able to conclude that, through the constructions presented, humans act like linear mass-spring-damper systems for the outputs being considered. This conclusion coincides with, and extends, research that shows the behaviours of some joints (and specifically the stance knee) act as mass-spring-damper systems when walking (Shamaei and Dollar, 2011; Scarfogliero and Folgheraiter, 2004) as well as additional research on animal legged locomotion (Holmes et al., 2006) showing that various types of legged locomotion appear to have a simple mathematical explanation: a reduced order method of simple gait generation buried under the complex neuromuscular system.

Step 3 constitutes controller construction utilising human outputs represented with canonical walking functions. For each of the six output combinations studied in this paper, a *human-inspired controller* will be constructed which yields stable human-like bipedal robotic walking through a *human-inspired optimisation*. The presence of discrete output data which express the human walking gait in a fashion qualitatively compatible with the canonical human functions naturally leads one to consider an optimisation problem that produces the best fit of the canonical walking functions to the human output data. Similar methods have been employed in the literature (Brubaker and Fleet, 2008; Olenšek and Matjačić, 2007), however, the parameters that result from solving such an unconstrained optimisation problem do not necessarily result in robotic walking and, moreover, certainly do not guarantee stability in any formal manner. The desire to have formal stability motivates the addition of constraints to the optimisation problem; this paper will show precisely the conditions necessary to constrain the optimisation problem in order to guarantee formal stability of designed walking gaits. Adding constraints to the optimisation problem will in general reduce the optimality of the fits; however, it is shown in this paper that the correlations of the fits are still very near unity. This is a very important observation as it indicates that both passive dynamics and mechanical design play an integral role in human walking. In order to quantify the human-like nature of the gait, the kinematics will be compared with human walking and it will be shown that the generated gaits typically lie within the range of healthy human walking as defined in Perry and Burnfield (2010) — this motivates the term *human-inspired optimisation*.

The human-like nature of the robotic walking obtained in this paper is especially remarkable for two reasons. First, the human-inspired control method, by virtue of the use of canonical walking functions, sheds light on the complex dynamics of human walking by providing a simplified 'black box' model while still capturing the fundamental mechanisms underlying human walking. Indeed, analysis of the canonical functions representing human outputs indicates that these outputs exhibit the characteristics of linear mass-spring-damper systems at the most basic level. Moreover, of these functions, the one representing the stance knee corresponds to a stable mass-spring-damper (there is a positive damping ratio) while all of the other outputs correspond to unstable mass-spring-dampers (with negative damping ratios). Thus, during the course of a step, humans absorb energy through the stance knee and compensate for energy loss by adding energy to the other joints. The second notable conclusion from the results presented is a consequence of the dramatic differences between humans and the robotic models considered in this paper; whereas a human is a complex dynamical system, the robotic model under study in this paper consists of only four links with point feet and walks in 2D. Yet, despite these somewhat dramatic physical differences, human-inspired control nonetheless results in human-like walking on bipedal robotic models with minimal difficulty in terms of implementation. This modelling analogy is achieved through the use of the 'black box' modelling paradigm of human walking – the robots and humans have very different dynamics due to the modelling differences. By analysing walking in terms of input/output behaviour, human-inspired control provides a method for obtaining robotic walking by driving the outputs of the robot to act like the outputs of the human. This second conclusion will be supported by simulation results, both on a robot with 'human-like' parameters and on a robot with parameters which are comparatively dissimilar to those of a human.

1.2 Related work

Bipedal robotic walking is a multidisciplinary research field that involves both biomechanics and robotics. As a result, the application of research in bipedal robotics is far-reaching; it can be applied to prosthetic design (Kumar et al., 2010), orthotic design and testing (Popovic et al., 2004) as well as space exploration (Ambrose et al., 2000). In order to create normal walking with a powered prosthesis

or orthosis, it is necessary to mimic the behaviour of human walking (Torrealba et al., 2008; Glaister et al., 2009). The prosthetis is also required to exhibit a dynamics that is similar to that of a human (Au and Herr, 2008; Ogura et al., 2006). Most controllers for prostheses and orthoses are implemented by using human data (Grimes et al., 1977; Popović et al., 1991). Not only the position but also the energy and force are considered to match human data, and different sensors are employed to measure all those variables (Herr and Wilkenfeld, 2003; Martinez-Villalpando et al., 2008). However, if human-like bipedal robotic walking is achieved and human walking can be predicted by the canonical walking functions, the force and energy can be calculated directly from the position data, which will greatly reduce the cost of the devices and simplify the controller design.

In the field of biomechanics, research related to human walking tends to focus on five major aspects: motion analysis, dynamic electromyography (EMG), force plate analysis, stride analysis and energy expenditure (Perry and Burnfield, 2010). Motion analysis uses joint movements to describe walking behaviours (Nyan et al., 2008; Kumar et al., 2010; Deluzio, 1997). Dynamic EMG is employed to identify muscle functionality (Bojanic et al., 2011; Cifrek et al., 2009). Force plate analysis emphasises ground reaction forces, moments of force, and power (Watt et al., 2010; Wong et al., 2010). These three methods are based on the specific events which constitute the act of walking, while stride analysis (Zampeli et al., 2010; Ko et al., 2009) and energy expenditure (Rand et al., 2009; Kramer, 2010; Kuo, 2007) are used in distinguishing normal waking gaits and pathological gaits. The hope is that this work, because of its emphasis on kinematic analysis, may aid in determining the differences between normal and pathological gaits without implicit knowledge of the internal dynamics.

Robotic researchers make an effort to use the research results from biomechanics where human walking has been extensively studied. However, due to the limitations of robot design, it can be quite challenging to ascertain the relationship between inputs and outputs in the motor control system from EMG and muscle force. Among the five aspects of human walking analysis in biomechanics, motion analysis is essentially the only method that can be applied to robot design. Most robot designs place the actuators at each joint (Deluzio, 1997); these actuators are used to make the joints follow certain selected trajectories fitted from human data (Srinivasan et al., 2008, 2009). These designs basically rely on tracking human data from one specific human subject. The tracked variables are chosen randomly. In addition, there is no quantitative comparison between the bipedal walking and human walking.

Bipedal robotic walking has been extensively studied from a variety of perspectives. Although there have been a few studies that directly relate human walking to robotic walking (Srinivasan et al., 2008, 2009), this connection has not been made in a fashion that proves robust and extensible. The hope is that this work will lay the groundwork for true human-like robotic walking, where human walking data form a basis for formal controller design. Building robots that exhibit human-like walking has long since drawn the attention of both the public and researchers alike (Kuo, 2002; Schaub et al., 2009; Srinivasan et al., 2008, 2009). Though dynamic robotic walking has been achieved in numerous cases in simulation (Ames et al., 2009; Spong and Bullo, 2005) and experiment (McGeer, 1990; Westervelt et al., 2007; Yadukumar et al., 2012; Sinnet and Ames, 2012), when looking at current walking robots, it is clear that humanlike walking has yet to be obtained.

1.3 Paper structure

The rest of this paper is structured in the following manner: in Section 2, the experimental setup and data processing are described. The human outputs considered in this paper [as chosen according to criteria (OC1-3)] are introduced in this section and computed from the experimental walking data. Finally, the *canonical walking functions* are introduced, and it is demonstrated that these time-dependent functions accurately describe the human output data. The robotic model, consisting of a 2D biped with knees and point feet, is developed in Section 3; specifically, hybrid systems are introduced, and it is shown how the robot considered in this paper is modelled by systems of this form. In Section 4, the human-inspired control law is constructed; this drives the outputs of the robot to the output of the human. Moreover, an optimisation problem is introduced in this section in order to determine the parameters of this control law such that the best fit of the human data is provided while still producing stable robotic walking. This is supported by simulation results in Section 5 which verify the human-like nature of the robotic walking that is achieved. In addition, results of considering different output combinations are illustrated and a criterion is provided to find the best output combination, i.e., the output combination that results in the 'most' human-like robotic walking. The final technical section of this paper, Section 6, shows the extensibility of the presented procedure by applying it to the model of a real physical robot (with parameters that are much different than those of a human). Finally, some conclusions are given in Section 7.

2 Human walking analysis

This section presents the method for human data collection, the human output functions considered as computed from the data, and introduces canonical walking functions that will be fit to the data – these will demonstrate that, for the outputs chosen, humans act like linear mass-spring-damper systems. For each of the various experimental trials, the data from one step cycle will be isolated. Twelve outputs on the kinematics of the data will be considered subject to the criteria (OC1-3) for valid human outputs posited in the introduction; averaging between all subjects with respect to each output is used to mitigate dependence on subject-to-subject variations in parameters and gaits. The computed

human outputs are discrete in nature since they are obtained from motion capture. For the purposes of controller design, a time-dependent representation of these outputs is needed. Two canonical walking functions are considered which yield special insight into the behaviour of the human with respect to the output functions chosen; it is shown that these functions can be fit to the human data with correlation coefficient near unity. The canonical walking functions, therefore, help to reveal the fundamental kinematics of human walking while simultaneously serving as a way to utilise human outputs in robotic design.

2.1 Experimental setup

The dataset presented in this paper was collected using the phase space system. By strategically positioning 12 high-precision cameras to cover a room of size $5 \times 5 \times 5$ m^3 and 19 light emitting diodes (LEDs) on a test subject, it was possible to collect 3D spatial measurements with an accuracy of 1 mm at 480 frames per second. Specifically, eight LEDs were placed on each leg as in Figure 1; one LED was placed on the sternum, one on the back directly behind the sternum, and one on the umbilicus.

Figure 1 The experimental setup, (a) placement of the emitters on test subject; the walking path is in blue (b) leg emitter locations (see online version for colours)

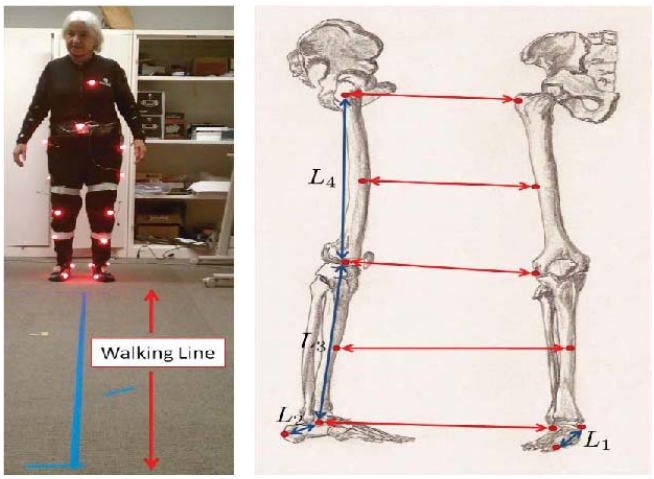

Each trial of the experiment required a subject to walk 3 m along a line at a normal speed on flat ground. Each subject performed 11 trials in a single experiment. Test subjects spanned a wide demographic spectrum: there were two female and seven male subjects with ages ranging between 17 and 30, heights ranging between 160.0 cm and 188.5 cm, and weights ranging between 47.7 kg and 90.9 kg. Table 1 provides the measurements of each subject. Note that the data were collected from two experiments separately. The data of the first five subjects were taken from one experiment and the data for the other four subjects were collected from an experiment one year later. The two experiments have the same setup and were conducted in the same lab. Though the data were collected from two experiments, the results of the analysis are the same, which shows that the data processing algorithm and the experimental results are repeatable.

2.2 Data analysis

The collection of experimental data was processed using three steps to make it suitable to analyse:

1 *Interpolation*. In order to resolve complications with self-occlusion – a phenomenon which occurs when a human test subject obscures one or more of the emitters – the effective walking period is isolated and interpolation is performed using cubic splines. This preprocessing results in relatively clean data over the course of a few step cycles. For each trial, at least two step cycles are isolated – one with each leg – to ensure that the data repeat. If the data are unusable, the trial is dropped.

2 *Rotation*. Using the preprocessed data, a series of rotations is then employed to ensure that walking occurs in the x-z plane, where x is the walking direction and z is the upright direction. This is achieved by examining the umbilical emitter of each subject which moves in an approximately linear fashion. The direction of the walking is determined by fitting a line to this forward evolution.

3 *Averaging*. Rather than smooth the data with aggressive filtering techniques, the trajectories of the emitters for every trial of a given subject are averaged. Under the assumption that test subjects walked at the same pace in all trials, the only additional processing required is to shift the data in time so the trials match up before averaging can be performed (Ames, 2011b). Only the datasets corresponding to the heels will be used to determine the beginning and end of each step cycle.

Figure 2 The data for the z position of one heel, p_{heel}, together with the acceleration, a_{heel} (see online version for colours)

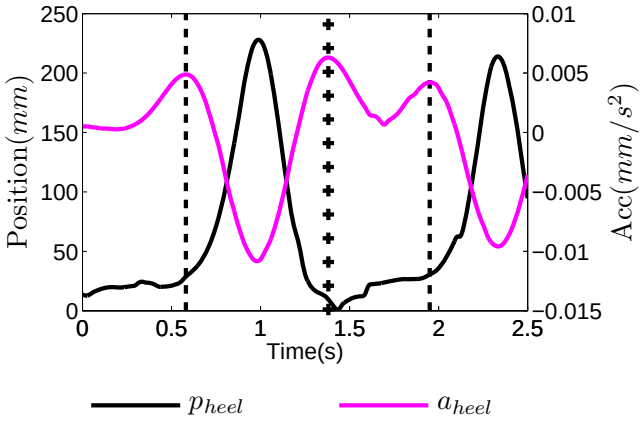

Notes: The line formed by – is the moment the heel lifts from the ground. The + line indicates the moment the heel strikes.

Table 1 Subjects from experiment

Subject	*Sex*	*Age*	*Ht. (cm)*	*Mass (kg)*	m_h *(kg)*	m_t *(kg)*	m_c *(kg)*	L_t *(cm)*	L_c *(cm)*
S_1	M	17	188.5	83.9	56.9	8.4	3.9	49.3	45.1
S_2	M	22	169.5	90.9	61.5	9.1	5.5	40.1	43.5
S_3	M	30	170.5	69.1	46.7	6.9	3.3	43.8	38.1
S_4	M	26	163.5	58.9	39.3	5.9	2.7	38.5	38.2
S_5	F	23	165.5	47.7	32.3	4.8	2.9	39.2	37.6
S_6	F	27	160.0	56.7	38.4	5.7	2.6	46.6	37.1
S_7	M	30	160.5	58.9	40.0	5.9	2.7	38.8	30.4
S_8	M	25	182.0	90.7	61.5	9.1	4.2	49.5	40.1
S_9	M	22	173.0	68.0	46.1	6.8	3.2	59.2	35.6
$\overline{S}$	*	*	170.3	69.4	47.1	6.9	3.2	45.2	38.1

Notes: The subject number is in the left column and the L_c, L_t, m_c, m_t measurements correspond to the lengths described in Figure 3(b). The measurements m_c and m_t are calculated according to the mass distribution in Winter (1990)

Since human-walking is naturally periodic and symmetric, it is sufficient to characterise a walking gait by examining only one step cycle, ranging from heel strike of one leg to heel strike of the other. Therefore, data from only one step cycle are used. The relevant data are isolated by determining the moment at which the heel strikes the ground, i.e., the pattern transition moment. The heel strike time is determined based on observation of the acceleration in the z direction. The acceleration, which is the second order difference of the heel height, attains maxima when the heel strikes the ground and when the heel lifts from the ground. Figure 2 shows both the position and acceleration of the heel along with vertical lines indicating when heel strike and heel lift occur.

There are two reasons why toe behaviour is not considered in this work. First, heel strike represents the main impact from the whole human walking system. Compared with toe behaviour, the heel behaviour is more important to human walking analysis. Second, the bipedal robot considered in this paper has point feet. Human heel-strike is analogous to foot-strike for such a robot.

2.3 Human outputs

The mean human (MH) datasets found through the above procedure are used to search for human kinematics outputs satisfying the three output criteria (OC1-3) mentioned in Section 1. Motivated by the apparent decoupling of the sagittal and coronal dynamics in human walking (Ames et al., 2007), this paper focuses solely on walking in the sagittal plain forgoing analysis of the coronal plane. It is quite common in the literature to make this assumption and doing so enables the use of a 2D robotic model. As such, this study is restricted to the principle angles responsible for walking in the sagittal plane (Perry and Burnfield, 2010) [see Figure 3(a)] consisting of the angle the stance calf makes with the vertical, θ_{sa}, and the relative angles between the links, θ_{sk}, θ_{hip}, and θ_{nsk}, as follows: $\boldsymbol{\theta} = (\theta_{sa}, \theta_{sk}, \theta_{hip}, \theta_{nsk})$.

Figure 3 (a) Configuration variables (human joint angles) and (b) mass/length distribution

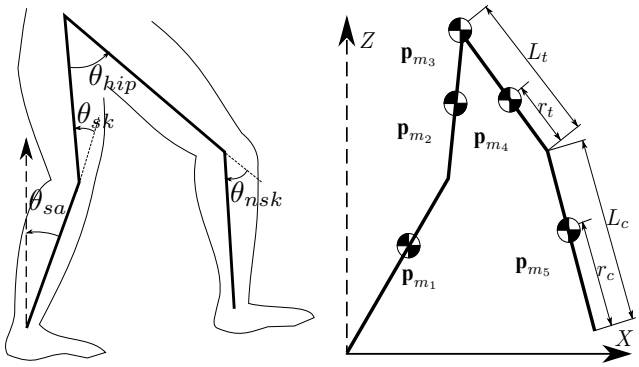

(a) (b)

Notes: The masses are $m_1 = m_5 = m_c$, $m_2 = m_4 = m_t$, and $m_3 = m_h$; see Table 1.

Figure 4 The human output functions based upon the (a) position of the hip and (b) the position of the CoM; in both cases, the outputs chosen result in a compass-gait representation (see online version for colours)

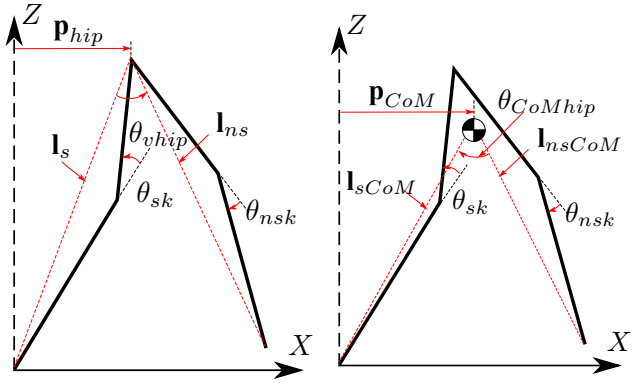

(a) (b)

The desired human outputs should be functions of these angles, have 'simple' time-dependent representations, and be mutually exclusive. In essence, these conditions imply that the human outputs must have a one-to-one correspondence with the joint angles, while simultaneously being 'simple' functions of time. Twelve different output functions are found which satisfy these requirements; they are shown in Figure 4. These outputs will be listed shortly, but first, some variables will be introduced to simplify the output descriptions. Let

$$\mathbf{l}_s = \mathbf{p}_{nsf} - \mathbf{p}_{hip}, \tag{1}$$

$$\mathbf{l}_{ns} = \mathbf{p}_{sf} - \mathbf{p}_{hip}, \tag{2}$$

be vectors representing the virtual stance and non-stance legs [as in Figure 4(a)] oriented from the hip toward the ankles; here $\vec{p}_{sf}$ is the position of the stance foot in the x-z plane, $\vec{p}_{hip}$ is the position of the hip, and $\vec{p}_{nsf}$ is the position of the non-stance foot. Similarly, let

$$\mathbf{l}_{sCoM} = \mathbf{p}_{nsf} - \mathbf{p}_{CoM}, \tag{3}$$

$$\mathbf{l}_{nsCoM} = \mathbf{p}_{sf} - \mathbf{p}_{CoM}, \tag{4}$$

represent the virtual stance and non-stance legs [as in Figure 4(b)] oriented from the CoM toward the ankles, with

$$\mathbf{p}_{CoM} = \frac{1}{\sum_{i=1}^{5} m_i} \sum_{i=1}^{5} m_i \mathbf{p}_{m_i}, \tag{5}$$

where m_i represents the mass of point mass i and $\mathbf{p}_{m_i}$ represents the x-z position of point mass i [see Figure 3(b)]. The outputs can now be described where forward kinematics may be used to find the quantities specified:

O1 The x-position of the hip, $p_{hip} = (\mathbf{p}_{hip})_x$.

O2 The x-position of the CoM, $p_{CoM} = (\mathbf{p}_{CoM})_x$.

O3 The angle of the stance knee, θ_{sk}.

O4 The length of the virtual leg connecting the hip to the stance ankle, $\ell_s = \| \mathbf{l}_s \|$.

O5 The length of the virtual leg connecting the CoM to the stance ankle, $\ell_{sCoM} = \| \mathbf{l}_{sCoM} \|$.

O6 The slope of the non-stance leg, i.e., the tangent of the angle between the z-axis and the line connecting the non-stance ankle and hip, as shown in Figure 4,

$$m_{nsl} = \frac{(\mathbf{l}_{ns})_x}{(\mathbf{l}_{ns})_z}. \tag{6}$$

O7 The angle between the virtual legs connecting the hip to the ankles,

$$\theta_{vhip} = \cos^{-1}\left(\frac{\mathbf{l}_s \cdot \mathbf{l}_{ns}}{\|\mathbf{l}_s\| \|\mathbf{l}_{ns}\|} \right), \tag{7}$$

where $\mathbf{l}_s$ and $\mathbf{l}_{ns}$ are vectors representing the stance and non-stance virtual legs, respectively, as shown in Figure 4(a).

O8 The slope of the virtual leg connecting the CoM to the non-stance ankle,

$$m_{nsCoM} = \frac{(\mathbf{l}_{nsCoM})_x}{(\mathbf{l}_{nsCoM})_z}. \tag{8}$$

O9 The angle between the virtual legs connecting the ankles to the CoM,

$$\theta_{CoMhip} = \cos^{-1}\left(\frac{\mathbf{l}_{sCoM} \cdot \mathbf{l}_{nsCoM}}{\|\mathbf{l}_{sCoM}\| \|\mathbf{l}_{nsCoM}\|} \right). \tag{9}$$

O10 The angle of the non-stance knee, θ_{nsk}.

O11 The length of the virtual leg connecting the hip to the non-stance ankle, $\ell_{ns} = \| \mathbf{l}_{ns} \|$.

O12 The length of the virtual leg connecting the CoM to the stance ankle, $\ell_{nsCoM} = \| \mathbf{l}_{nsCoM} \|$.

To better understand the motivation behind these choices of outputs, note that the outputs considered essentially represent the human (and later a robot) as a compass-gait biped (Espiau and Goswami, 1994; Goswami et al., 1998) with telescoping legs. In particular, two separate compass-gait biped representations are considered:

1 a compass-gait defined about the position of the hip defined by outputs O1, O4, O6 or O7, and O11 as shown in Figure 4(a)

2 a compass-gait biped defined about the position of the CoM as defined by outputs O2, O5, O8 or O9, and O12 as shown in Figure 4(b).

The other outputs, O3 and O10, i.e., the angles of the knees, are also considered due to their intuitive nature and the importance that knees play in bipedal walking. Also note that the knee angles can be related to the lengths of the stance and non-stance legs through simple trigonometric identities, thus fitting within the conceptual picture of representing the human and/or robot as a compass-gait biped.

Each of the mentioned outputs coarsely corresponds to one of the system's angles. To summarise, these outputs can be partitioned into four disjoint sets:

$$Y_{sa} = \{ p_{hip}, p_{CoM} \}, \tag{10}$$

$$Y_{sk} = \{ \theta_{sk}, \ell_s, \ell_{sCoM} \}, \tag{11}$$

$$Y_{hip} = \{ m_{nsl}, \theta_{vhip}, m_{nsCoM}, \theta_{CoMhip} \}, \tag{12}$$

$$Y_{nsk} = \{ \theta_{nsk}, \ell_{ns}, \ell_{nsCoM} \}. \tag{13}$$

It is easy in most cases to see that each of these sets has a one-to-one correspondence with the joint angles of the human, with the correspondence given by:

$$Y_{sa} \leftrightarrow \theta_{sa}, Y_{sk} \leftrightarrow \theta_{sk}, Y_{hip} \leftrightarrow \theta_{hip}, Y_{nsk} \leftrightarrow \theta_{nsk}. \quad (14)$$

These correspondences imply that outputs from distinct sets are mutually exclusive, indicating that the decoupling matrix used in feedback linearisation associated with outputs chosen from each set is full rank (Ames, 2011b) (this will be discussed further and used in the design of controllers in Section 4).

Figure 5 The human output sets Y_{sa}, Y_{sk}, Y_{hip}, and Y_{nsk} as computed from the MH data over one step and the canonical walking functions fitted to these data; here the time of a step is normalised to one, (a) stance ankle outputs – Y_{sa} (b) stance knee outputs – Y_{sk} (c) hip outputs – Y_{hip} (d) non-stance knee outputs – Y_{nsk} (see online version for colours)

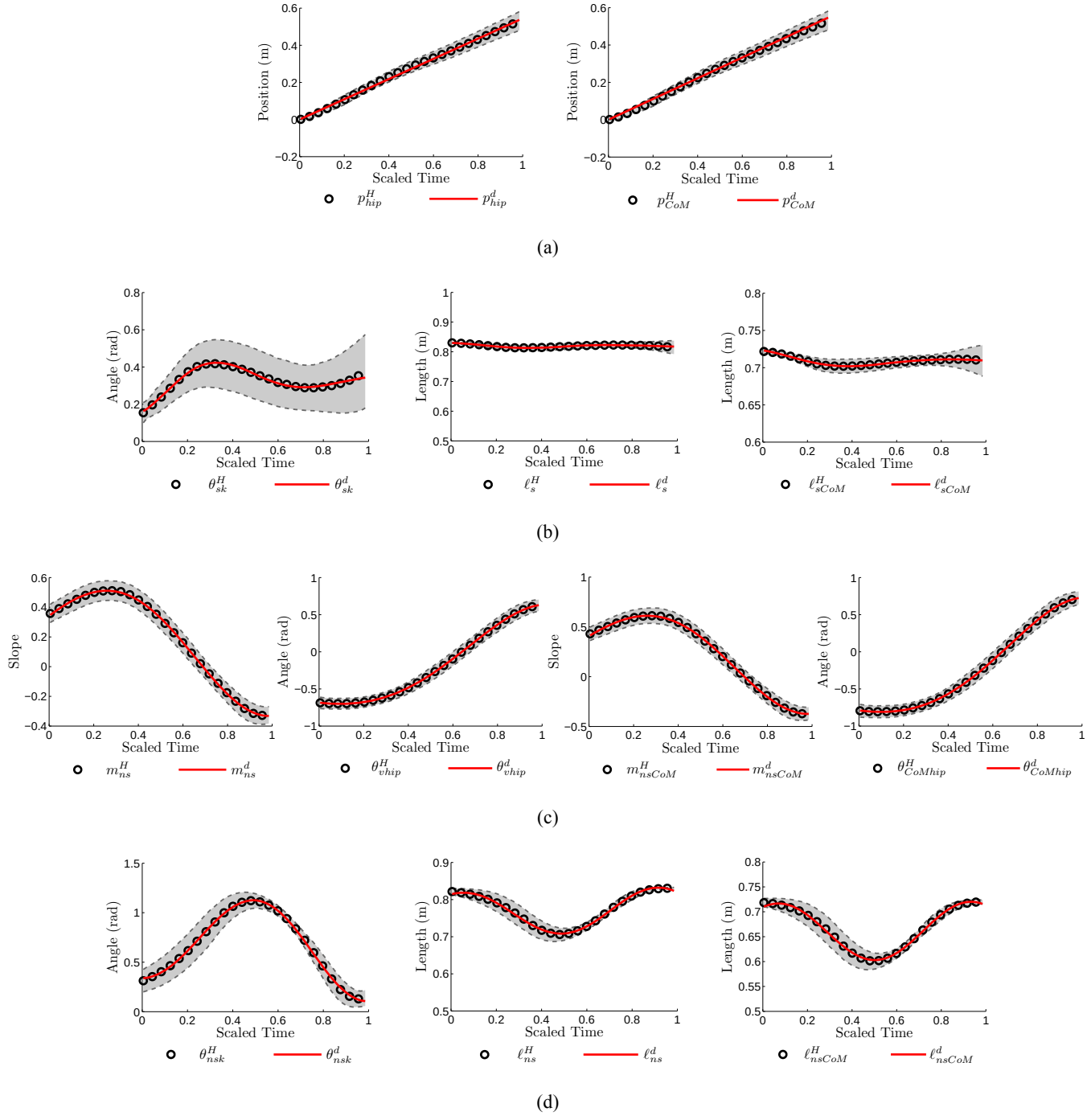

Notes: The plotted human data for each output (black) are denoted with superscript *H* and the error bands show one standard deviation from the mean. The fits of the canonical walking functions to the human data are shown in red and denoted with superscript *d*.

Each of the 12 outputs is computed from the human data over the course of a single step by:

1 normalising the step time of each subject to one

2 resampling the data so that all subjects shared sampling frequency f_s

3 averaging the data for each sample time $t = k/f_s$ for $k \in \{1, 2, \ldots, K\}$ with K the number of samples.

The mean of these outputs for the nine subjects is computed and shown in Figure 5 along with one standard deviation (1σ) from this mean. According to Perry and Burnfield (2010), outputs that lie within the 1σ error bands are representative of normal walking. This metric provides a practical method for determining when bipedal robots display 'human-like' walking.

2.4 Canonical walking functions

After obtaining the MH outputs, it is necessary to represent them as time-dependent functions in order to parameterise these functions over the course of a step. Doing so will allow for controller design on the continuous dynamics of the system. Thus, simple functions – termed *canonical walking functions* – are fit to the discrete data to enable controller design.

Inspection of the human data for Y_{sa} in Figure 5 indicates that both the position of the hip and the position of the CoM, p_{hip} and p_{CoM}, respectively, can be accurately described by a linear function of time:

$$y_1^H = vt. \tag{15}$$

Performing a least squares fit of this function to the human output data for p_{hip} and p_{CoM} confirms that this function provides a valid characterisation of the human data with respect to these two outputs. In particular, (15) can be fit to the human data with a correlation of 0.999 (see Table 2) providing a near-perfect time-dependent representation. It is important that the positions of the hip and CoM are linear in time as this observation implies that humans walk at a constant pace with velocity v. This will prove useful both in defining a parameterisation of time based upon the position of the hip or CoM (to be introduced in Section 4) and directly controlling the walking speed of a robot by constraining this parameter (as will be discussed in Section 6).

Upon reviewing the human outputs comprising the sets Y_{sk}, Y_{hip}, and Y_{nsk} in Figure 5, it appears that a sinusoidal behaviour is exhibited with possible exponential decay. This observation naturally leads to the time solution to a linear mass-spring-damper system as a means of characterising human outputs – especially considering that the knee behaviour of humans when walking has been shown to be described by a linear mass-spring-damper system (Shamaei and Dollar, 2011). The solution to such a system satisfies

$$y = e^{-\xi\omega_n t}\left(c_0\cos(\omega_d t) + c_1\sin(\omega_d t)\right) + \hat{g}, \tag{16}$$

where ξ is the damping ratio, ω_n is the natural frequency and $\omega_d = \sqrt{1-\xi^2}\,\omega_n$ is the damped natural frequency, c_0 and c_1 are parameters determined by the initial position, $y(0)$, and the initial velocity, $\dot{y}(0)$, and $\hat{g}$ is a constant that results from gravity acting on the system. Motivated by (16), define the second canonical function as:

$$y_2^H = e^{-\alpha_4 t}\left(\alpha_1\cos(\alpha_2 t) + \alpha_3\sin(\alpha_2 t)\right) + \alpha_5. \tag{17}$$

Comparing (16) and (17), one sees that $\alpha_1 = c_0$, $\alpha_2 = \omega_d$, $\alpha_3 = c_1$, $\alpha_4 = \xi\,\omega_n$ and $\alpha_5 = \hat{g}$.

Table 2 Parameter values of the canonical walking functions for the MH outputs together with the correlations of the least squares fits

Output set	*Outputs*	$y_1^H = vt,\ y_2^H = e^{-\alpha_4 t}\left(\alpha_1\cos(\alpha_2 t) + \alpha_3\sin(\alpha_2 t)\right) + \alpha_5$						
		v	α_1	α_2	α_3	α_4	α_5	*Cor.*
$Ysa \leftrightarrow \theta_{sf}$	p_{hip}	0.9143	*	*	*	*	*	0.9990
	p_{CoM}	0.9314	*	*	*	*	*	0.9993
$Y_{sk} \leftrightarrow \theta_{sk}$	θ_{sk}	*	–0.1739	13.6644	0.0397	3.3222	0.3332	0.9934
	ℓ_s	*	0.0106	14.6144	−0.0001	2.5168	0.8193	0.9891
	ℓ_{sCoM}	*	0.0148	11.9444	–0.0020	3.4513	0.7085	0.9955
$Y_{hip} \leftrightarrow \theta_{hip}$	m_{nsl}	*	0.1577	7.2712	0.2317	–1.0613	0.1847	0.9999
	θ_{vhip}	*	–0.2723	–5.6926	–0.0177	–2.3414	–0.4125	1.0000
	m_{nsCoM}	*	0.1753	7.3371	0.2705	–1.1019	0.2329	0.9998
	θ_{CoMhip}	*	–0.2880	–5.7885	–0.0195	–2.5533	–0.5009	1.0000
$Y_{nsk} \leftrightarrow \theta_{nsk}$	θ_{nsk}	*	–0.3439	10.5728	0.0464	–0.8606	0.6812	0.9996
	ℓ_{ns}	*	0.0476	12.2755	0.0186	–0.4545	0.7666	0.9985
	ℓ_{nsCoM}	*	0.0487	12.2312	0.0270	–0.1166	0.6606	0.9986

The capacity of the canonical function (17) to accurately describe the human output data for the outputs comprising the sets Y_{sk}, Y_{hip}, and Y_{nsk} can be determined by examining a least squares fit of this function to the human output data; this fit is shown in Figure 5 and, in particular, it can be seen that there is very good agreement between the human data and the canonical function (17). This purported visual agreement can be substantiated by considering the correlation coefficients of these fits as given in Table 2, where all of the correlations are greater than 0.99. These near-unity correlations imply that the function (17) accurately describes the human output data for the functions choices considered in this paper. Moreover, this alludes to an important phenomenon present in human walking: for the outputs chosen, humans act like a *linear* mass-spring-damper system despite the complexity of unknown, non-linear internal dynamics. This conclusion provides support to current work in the field of prosthetics where spring-damper systems are used to mimic human muscle behaviours (Morgenroth et al., 2011; Bellmann et al., 2010).

The representation of human walking as a linear mass-spring-damper system allows one to draw important conclusions about the nature of human walking. From Table 2, one can see that α_4 of (17) is negative for outputs O6-12 which correspond to sets Y_{hip} and Y_{nsk}, respectively; thus these outputs are governed by unstable mass-spring-damper systems which leads one to conclude that humans inject energy into the walking system; the total injected energy must be equal to the combination of the energy removed through control and the energy lost due at impact. Similarly, the outputs O3-5 corresponding to set Y_{sk} have a positive α_4 constant, implying that the behaviour associated to these outputs is stable, and the system acts to absorb energy for these outputs. Thus, human walking is a delicate harmony between stable and unstable dynamics – a balancing act for which the end result is *dynamically* stable walking. Considering these insights into human walking, it becomes apparent that, to achieve human-like bipedal robotic walking, the walking should be dynamically stable rather than statically stable).

3 Robotic model

Bipedal walking robots naturally display continuous and discrete behaviour throughout the course of a step – the continuous behaviour occurs when the leg swings forward and the discrete behaviour occurs when the foot strikes the ground. It is, therefore, natural to model robots of this form using hybrid systems, which provides a formal model for systems that display such hybrid behaviour. This section, therefore, introduces the basic formalisms of hybrid systems along with the specific hybrid models obtained for the robot that will be considered in this paper.

3.1 Hybrid systems

Hybrid systems can be defined in many different ways depending on the level of generality needed to model a given robot (Ames et al., 2011; Sinnet and Ames, 2009; Grizzle et al., 2010; Westervelt et al., 2007). A definition specialised to the models under study is introduced below:

Definition 1: A hybrid control system is *a tuple*,

$$\mathscr{HC} = (\mathbf{X}, \mathbf{U}, \mathcal{S}, \mathbf{\Delta}, \mathbf{f}, \mathbf{g}), \tag{18}$$

where

- $\mathbf{X}$ is the *domain* with $\mathbf{X} \subseteq \mathcal{X}$ a smooth sub-manifold of the state space $\mathcal{X} \subseteq \mathbb{R}^n$
- $\mathbf{U} \subseteq \mathbb{R}^m$ is the admissible control
- $\mathcal{X} \subset \mathbf{X}$ is a proper subset of $\mathbf{X}$ called the *guard* or *switching surface*
- $\Delta : \mathcal{S} \to \mathbf{X}$ is a smooth map called the *reset map*
- $(\mathbf{f}, \mathbf{g})$ is a *control system* on $\mathbf{X}$, i.e., $\dot{\mathbf{x}} = \mathbf{f}(\mathbf{x}) + \mathbf{g}(\mathbf{x})\mathbf{u}$.

A *hybrid system* is a hybrid control system with $\mathbf{U} = \emptyset$, i.e., any applicable feedback controllers have been applied, making the system closed-loop. In this case,

$$\mathscr{H} = (\mathbf{X}, \mathcal{S}, \Delta, \mathbf{f}), \tag{19}$$

where $\mathbf{f}$ is a dynamical system on $\mathbf{X} \subseteq \mathcal{X}$, i.e., $\dot{\mathbf{x}} = \mathbf{f}(\mathbf{x})$.

3.2 Robotic models

In this paper, a two-dimensional robotic model with knees and feet is synthesised from human mass/length parameters; this human-like model is used in simulation. The model consists of four links leading to configuration space $\mathcal{Q}$ with coordinates: $\boldsymbol{\theta} = (\theta_{sa}, \theta_{sk}, \theta_{hip}, \theta_{nsk})^T$, as displayed in Figure 3(a). Since the robotic model has only point feet, the stance foot angle – the angle between the foot and the vertical – is the same as the stance ankle angle, θ_{sa}, in the human model as shown in Figure 3(a). The remaining coordinates are: θ_{sk}, the angle of the stance knee, θ_{hip}, the angle of the hip, and θ_{nsk}, the angle of the non-stance knee. The mass placement of the model is shown in Figure 3(b).

Motivated by the goal of achieving human-like robotic walking on a human-like robot, this paper attempts to closely mimic a human with respect to mass placement in the fabrication of the human-like model as this will result in a viable comparison between human data and robot behaviour. The mass and length parameters of the human model are taken to be the averaged value of the all subjects in the experiments, which can be found in the Table 1 as $\overline{S}$. In order to strengthen the experimental results, a second model, AMBER, is considered which is less human-like than the first model; in particular, the model for AMBER is obtained from the parameters of a real physical robot (see Figure 6). The reader will see that the methods outlined in this paper result in successful robotic walking in simulation (Section 6), thus showing the utility for robotic walking platforms.

The hybrid model of this system is represented as a tuple:

$$\mathscr{HC}_R = (\mathbf{X}, \mathbf{U}, \mathcal{S}, \boldsymbol{\Delta}, \mathbf{f}, \mathbf{g}). \tag{20}$$

Figure 6 (a) The robot AMBER and (b) its model in SolidWorks (see online version for colours)

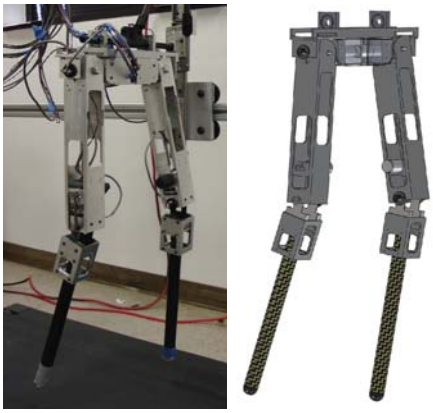

(a) (b)

3.2.1 Continuous dynamics

The continuous dynamics can be derived using a Lagrangian which depends on the configuration variable $\boldsymbol{\theta}$ and the mass/length parameters:

$$L(\boldsymbol{\theta}, \dot{\boldsymbol{\theta}}) = \frac{1}{2}\dot{\boldsymbol{\theta}}^T \mathbf{D}(\boldsymbol{\theta})\dot{\boldsymbol{\theta}} - V(\boldsymbol{\theta}), \tag{21}$$

where $\mathbf{D}(\boldsymbol{\theta})$ is a manipulator inertia matrix and $V(\boldsymbol{\theta})$ is the potential energy. The Euler-Lagrange equation yields the dynamic model

$$\mathbf{D}(\boldsymbol{\theta})\ddot{\boldsymbol{\theta}} + \mathbf{H}(\boldsymbol{\theta}, \dot{\boldsymbol{\theta}}) = \mathbf{B}(\boldsymbol{\theta})\mathbf{u}, \tag{22}$$

where $\mathbf{B}(\boldsymbol{\theta})$ is a torque distribution matrix which is full rank under the proper choice of coordinates, and $\mathbf{H}(\boldsymbol{\theta}, \dot{\boldsymbol{\theta}})$ is

$$\mathbf{H}(\boldsymbol{\theta}, \dot{\boldsymbol{\theta}}) = \mathbf{C}(\boldsymbol{\theta}, \dot{\boldsymbol{\theta}})\dot{\boldsymbol{\theta}} + \mathbf{G}(\boldsymbol{\theta}), \tag{23}$$

with $\mathbf{C}(\boldsymbol{\theta}, \dot{\boldsymbol{\theta}})$ containing terms resulting from the Coriolis effect and centripetal acceleration and $\mathbf{G}(\boldsymbol{\theta}) = dV(\boldsymbol{\theta})$ containing terms resulting from gravity. The dynamic model can be written as the affine control system $(\mathbf{f}, \mathbf{g})$ where

$$\mathbf{f}(\boldsymbol{\theta}, \dot{\boldsymbol{\theta}}) = \begin{bmatrix} \dot{\boldsymbol{\theta}} \\ -\mathbf{D}^{-1}(\boldsymbol{\theta})\mathbf{H}(\boldsymbol{\theta}, \dot{\boldsymbol{\theta}}) \end{bmatrix}, \mathbf{f}(\boldsymbol{\theta}) = \begin{bmatrix} \mathbf{0} \\ \mathbf{D}^{-1}(\boldsymbol{\theta})\mathbf{B}(\boldsymbol{\theta}) \end{bmatrix}. \tag{24}$$

Under the choice of coordinates used in this paper, $\mathbf{B}(\boldsymbol{\theta}) = \mathbf{I}_4$ is the identity matrix, and, under the assumption of full actuation, $\mathbf{U} = \mathbb{R}^4$.

3.2.2 Transition dynamics

The domain specifies the allowable configuration of the system as determined by a unilateral constraint $h(\boldsymbol{\theta})$; for the bipeds under study, this function specifies that the non-stance foot must be above the ground, i.e., $h(\boldsymbol{\theta}) > 0$ is the height of the non-stance foot. This leads to the following definition of the domain $\mathbf{X}$:

$$\mathbf{X} = \left\{(\boldsymbol{\theta}, \dot{\boldsymbol{\theta}}) \in \mathcal{X} : h(\boldsymbol{\theta}) \geq 0\right\}. \tag{25}$$

The guard is then just the boundary of the domain with the additional assumption that $h(\boldsymbol{\theta})$ is decreasing:

$$\mathcal{S} = \left\{(\boldsymbol{\theta}, \dot{\boldsymbol{\theta}}) \in \mathcal{X} : h(\boldsymbol{\theta}) = 0 \text{ and } dh(\boldsymbol{\theta})\dot{\boldsymbol{\theta}} < 0\right\}, \tag{26}$$

with dh the Jacobian of h. From this definition, one can see that the system hits the guard at the moment that the non-stance foot strikes the ground.

3.2.3 Discrete dynamics

The discrete dynamics of the robot determines how the velocities of the robot change when the foot impacts the ground while simultaneously switching the 'stance' and 'non-stance' legs. This dynamic model represents the reset map $\boldsymbol{\Delta}$ and is given by:

$$\boldsymbol{\Delta} : \mathcal{S} \to \mathbf{X}, \qquad \boldsymbol{\Delta}(\boldsymbol{\theta}, \dot{\boldsymbol{\theta}}) = \begin{bmatrix} \boldsymbol{\Delta}_{\boldsymbol{\theta}}\boldsymbol{\theta} \\ \boldsymbol{\Delta}_{\dot{\boldsymbol{\theta}}}(\boldsymbol{\theta})\dot{\boldsymbol{\theta}} \end{bmatrix}, \tag{27}$$

where $\boldsymbol{\Delta}_{\boldsymbol{\theta}}$ is a relabelling map which switches the stance and non-stance leg at impact (by appropriately transforming the angles). Here, $\boldsymbol{\Delta}_{\dot{\boldsymbol{\theta}}}$ determines the change in velocity due to impact; for the sake of brevity, this paper forgoes a detailed discussion on impact dynamics, but details can be found in Grizzle et al. (2010), and Hürmüzlü and Marghitu (1994). In brief, the impact map is computed by augmenting the configuration space with extended coordinates which include the Euclidean position of the stance foot and then applying a perfectly plastic impact model which balances angular momentum and applies impulsive forces to halt the motion of the non-stance foot at impact. The shock is distributed through the system by the impact model and some energy is, in fact, lost and must be recovered (injected) through control.

4 Robotic controller design

This section uses the human outputs and their time-dependent representations – canonical walking functions – to construct a controller which drives the outputs of the robot to the outputs of the human. In addition, an optimisation problem is introduced to determine the parameters for the canonical walking functions which provide the best fit of the human walking data while simultaneously constraining the optimisation parameters such that stable robotic walking is achieved. This manner of matching kinematics provides a concrete manner for evaluating the human-like nature of a gait (Perry and Burnfield, 2010).

4.1 Robot outputs

Relative degree is an important concept in feedback linearisation which specifies how the inputs appear in the outputs; more specifically, it specifies which order of lie derivative is necessary to calculate a control law which

drives the robot outputs to the canonical walking functions. In this section, two types of relative degree outputs will be described. Later, it will be formally verified that the outputs specified have the relative degree claimed; see Sastry (1999) for a formal discussion on feedback linearisation.

4.1.1 Relative degree 1 (RD1) output

Recall that the outputs O1-2 which comprise the set Y_{sa} – specifically, the *x*-positions of the hip and CoM – are represented by linear functions of time (15). Because this determination was made based on the capacity of the human functions to fit human kinematics outputs, the implication is that hip and CoM velocities are essentially constant, say $\overline{v}$ (which comes from optimisation). For this output set, Y_{sa}, the goal, then, is to create a controller which drives the velocity of the robot hip or CoM to the optimised velocity, $\overline{v}$. Let $Y_{sa}^R = \{p_{hip}^R, p_{CoM}^R\}$ represent the kinematic maps described by O1-2 but as computed from the robotic model. Then, formally, the controller should drive $\dot{y}_{sa}^R \to \overline{v}$ for $y_{sa}^R \in Y_{sa}^R$. This represents a tracking problem, so define the actual and desired outputs, respectively, as

$$y_1^a\left(\boldsymbol{\theta}, \dot{\boldsymbol{\theta}}\right) = dy_{sa}^R(\boldsymbol{\theta})\dot{\boldsymbol{\theta}}, \quad y_1^d = \overline{v}, \tag{28}$$

where dy_{sa}^R is the Jacobian of $y_{sa}^R \in Y_{sa}^R$.

4.1.2 Relative degree 2 (RD2) outputs

The remaining three output combinations, Y_{hip}, Y_{sk}, and Y_{nsk}, along with the canonical function (17) will form the basis for the RD2 outputs of the robotic system. The kinematic maps O3-12 can be applied to the robot by calculating them using the mass and length parameters of the robot, let the output sets be written as:

$$Y_{sk}^R = \left\{\theta_{sk}^R, \ell_s^R, \ell_{sCoM}^R\right\}, \tag{29}$$

$$Y_{hip}^R = \left\{m_{nsl}^R, \theta_{vhip}^R, m_{nsCoM}^R, \theta_{CoMhip}^R\right\}, \tag{30}$$

$$Y_{nsk}^R = \left\{\theta_{nsk}^R, \ell_{ns}^R, \ell_{nsCoM}^R\right\}. \tag{31}$$

The goal of the human-inspired controller construction is to drive an element from each of these sets to the appropriate canonical walking functions (17). Therefore, define the actual and desired outputs:

$$\mathbf{y}_2^a(\boldsymbol{\theta}) = \begin{bmatrix} y_{sk}^R(\boldsymbol{\theta}) \\ y_{hip}^R(\boldsymbol{\theta}) \\ y_{nsk}^R(\boldsymbol{\theta}) \end{bmatrix}, \mathbf{y}_2^d(t) = \begin{bmatrix} y_{sk}^d\left(t, \boldsymbol{\alpha}_{sk}\right) \\ y_{hip}^d\left(t, \boldsymbol{\alpha}_{hip}\right) \\ y_{nsk}^d\left(t, \boldsymbol{\alpha}_{nsk}\right) \end{bmatrix}, \tag{32}$$

with $y_{sk}^R \in Y_{sk}^R$, $y_{hip}^R \in Y_{hip}^R$, and $y_{nsk}^R \in Y_{nsk}^R$. In this case, y_2^d consists of the canonical walking functions (17). In other words, $y_{sk}^d(t, \boldsymbol{\alpha}_{sk}) = y_2^H(t, \boldsymbol{\alpha}_{sk})$, $y_{hip}^d(t, \boldsymbol{\alpha}_{hip}) = y_2^H(t, \boldsymbol{\alpha}_{hip})$, and $y_{nsk}^H(t, \boldsymbol{\alpha}_{nsk}) = y_2^H(t, \boldsymbol{\alpha}_{nsk})$ with $\boldsymbol{\alpha}_{sk}, \boldsymbol{\alpha}_{hip}, \boldsymbol{\alpha}_{nsk} \in \mathbb{R}^5$. Note that the parameters of these canonical walking functions could be chosen to be the parameters that resulted in the least squares fit of the human data, but this would not necessarily result in robotic walking. Therefore, a *human-inspired* optimisation will be posed that will determine the parameters of these functions that provide the best fit of the human data while ensuring robotic walking.

4.2 Controller design

By construction, human-like walking can be achieved when the actual outputs of the robot mimic the desired outputs, or

$$y_1^a = y_1^d \text{ and } \mathbf{y}_2^a = \mathbf{y}_2^d. \tag{33}$$

These criteria naturally lead one to consider feedback linearisation (also known as input/output linearisation), which provides a manner for driving the actual outputs to the desired outputs, or

$$y_1^a \to y_1^d \text{ and } \mathbf{y}_2^a \to \mathbf{y}_2^d \text{ as } t \to \infty. \tag{34}$$

One challenge stands in the way: the outputs are time-dependent, yet time-independence (autonomous state-dependence) tends to be more robust. Before using feedback linearisation to construct a controller, it is helpful to remove the time dependence from y_1^d and $\mathbf{y}_2^d$ using a parameterisation of time. Analysis of the *x*-positions of both the hip and the CoM indicate that these outputs are very nearly linear with respect to time, i.e., $y_{sa} \approx \overline{v}t$ for $y_{sa} \in Y_{sa}$, one has that that $t \approx \frac{y_{sa}}{\overline{v}}$. This motivates the following parameterisation of time:

$$\tau(\boldsymbol{\theta}) = \frac{y_{sa}^R(\boldsymbol{\theta}) - y_{sa}^R(\boldsymbol{\theta}^+)}{\overline{v}}, \tag{35}$$

which incorporates the *x*-position of the hip or CoM for the robot. Note that here $y_{sa}^R(\boldsymbol{\theta}^+)$ is the *x*-position of the hip or CoM of the robot at the beginning of a step (depending on which output is chosen, $y_{sa} \in Y_{sa}$), with $\boldsymbol{\theta}^+$ the configuration of the robot post-impact (i.e., at the beginning of a step). Applying the parameterisation (35) gives outputs:

$$y_1\left(\boldsymbol{\theta}, \dot{\boldsymbol{\theta}}\right) = y_1^a\left(\boldsymbol{\theta}, \dot{\boldsymbol{\theta}}\right) - y_1^d, \tag{36}$$

$$\mathbf{y}_2(\boldsymbol{\theta}) = \mathbf{y}_2^a(\boldsymbol{\theta}) - \mathbf{y}_2^d\left(\tau(\boldsymbol{\theta})\right). \tag{37}$$

Using these outputs, consider the following linearising feedback control law:

$$\mathbf{u}\left(\boldsymbol{\theta}, \dot{\boldsymbol{\theta}}\right) = -\mathbf{A}^{-1}\left(\boldsymbol{\theta}, \dot{\boldsymbol{\theta}}\right) \left(\begin{bmatrix} 0 \\ L_{\mathbf{f}}^2 \mathbf{y}_2\left(\boldsymbol{\theta}, \dot{\boldsymbol{\theta}}\right) \end{bmatrix} + \begin{bmatrix} L_{\mathbf{f}} y_1\left(\boldsymbol{\theta}, \dot{\boldsymbol{\theta}}\right) \\ 2\varepsilon L_{\mathbf{f}} \mathbf{y}_2\left(\boldsymbol{\theta}, \dot{\boldsymbol{\theta}}\right) \end{bmatrix} + \begin{bmatrix} \varepsilon y_1\left(\boldsymbol{\theta}, \dot{\boldsymbol{\theta}}\right) \\ \varepsilon^2 \mathbf{y}_2\left(\boldsymbol{\theta}, \dot{\boldsymbol{\theta}}\right) \end{bmatrix}\right), \tag{38}$$

where $\varepsilon \in \mathbb{R}^+$ is a control gain, $L_{\mathbf{f}} y$ represents the lie derivative of y along the vector field $\mathbf{f}$, and $\mathbf{A}$ is the decoupling matrix:

$$\mathbf{A}\left(\boldsymbol{\theta}, \dot{\boldsymbol{\theta}}\right) = \begin{bmatrix} L_{\mathbf{g}} y_1\left(\boldsymbol{\theta}, \dot{\boldsymbol{\theta}}\right) \\ L_{\mathbf{g}} L_{\mathbf{f}} \mathbf{y}_2\left(\boldsymbol{\theta}, \dot{\boldsymbol{\theta}}\right) \end{bmatrix}. \tag{39}$$

It is at this point that the full meaning of 'mutually exclusive' outputs, as given by a necessary condition on the human outputs (OC3) given in Section 1, becomes clear. It is exactly because the outputs were chosen to be mutually exclusive that the decoupling matrix $\boldsymbol{A}$ is non-singular over the range in which the robot operates. Furthermore, the output (36) is RD1 because it is a function of velocity and the outputs (37) are RD2 because they are position-dependent and do not contain velocity terms; see Sastry (1999). The control law (38) will drive $y_1^a \to y_1^d$ and $\mathbf{y}_2^a \to \mathbf{y}_2^d$ exponentially quickly at a rate determined by gain parameter ε, and thus, the outputs of the robot will match the desired human functions after a short time if ε is large enough.

Note that the control law (38) depends on both the parameter ε along with the parameters of the canonical walking functions $\overline{v}$, $\boldsymbol{\alpha}_{hip}$, $\boldsymbol{\alpha}_{sk}$ and $\boldsymbol{\alpha}_{nsk}$. Combining the parameters of the canonical walking functions into a single vector yields $\boldsymbol{\alpha} = (\overline{v}, \boldsymbol{\alpha}_{hip}, \boldsymbol{\alpha}_{sk}, \boldsymbol{\alpha}_{nsk}) \in \mathbb{R}^{16}$. With this notion, applying the control law (38) to the control system $(\mathbf{f}, \mathbf{g})$ given in (24) yields the vector field:

$$\mathbf{f}^{(\varepsilon,\boldsymbol{\alpha})}(\boldsymbol{\theta}, \dot{\boldsymbol{\theta}}) = \mathbf{f}(\boldsymbol{\theta}, \dot{\boldsymbol{\theta}}) + \mathbf{g}(\boldsymbol{\theta})\mathbf{u}(\boldsymbol{\theta}, \dot{\boldsymbol{\theta}}). \tag{40}$$

Finally, this vector field, when considered in conjunction with the hybrid control system modelling the bipedal robot $\mathcal{HC}_R$ yields a hybrid system:

$$\mathcal{H}_R^{(\varepsilon,\boldsymbol{\alpha})} = (\mathbf{X}, \mathcal{S}, \boldsymbol{\Delta}, \mathbf{f}^{(\varepsilon,\boldsymbol{\alpha})}), \tag{41}$$

which, again, is dependent on the parameters ε and $\boldsymbol{\alpha}$. Although the control law (38) that led to this hybrid system ensures that (33) is satisfied for the *continuous* dynamics of this hybrid system, it does not imply that robotic walking will be achieved due to the discrete dynamics of the hybrid system. This issue will be dealt with using the well-known concept of hybrid zero dynamics (Westervelt et al., 2003).

4.3 Human-inspired optimisation

In order to achieve robotic walking, the parameters, $\boldsymbol{\alpha}$, of the canonical walking functions must satisfy specific conditions. Simply solving for the best fit will result in very good fits, but these fits will not guarantee walking. The goal of this section is to formally define the conditions necessary for achieving walking gaits using the canonical walking functions found through optimisation. With this goal in mind, introduce a cost function for this optimisation, termed the *human-data-based* cost, dependent on the experimental human output data. Before formally defining this cost, it is necessary to introduce some notation. Recall that the outputs were divided into sets: Y_{sa}, Y_{hip}, Y_{sk} and Y_{nsk}. Let these sets be indexed by $I = \{sa, hip, sk, nsk\}$.

In particular, one can represent the data for each human output by $y_i^H[k]$ where $t^H[k]$ and $y^H[k]$ represent the time and human output data, respectively, with $k \in [1, ..., K] \subset \mathbb{Z}$ an index for the K data points. Then, define the human-data-based cost:

$$\text{Cost}_{\text{HD}}(\boldsymbol{\alpha}) = \sum_{k=1}^{K} \sum_{i \in I} \left(\beta_{y_i} \left(y_i^d \left(t^H[k], \boldsymbol{\alpha}_i \right) - y_i^H[k] \right)^2 \right). \tag{42}$$

where β_{y_i} represents weightings for each output; in this work, the reciprocal of the maximum and minimum value of the human data for a given output are used to weight that output. y_i with $i \in I$ are the four outputs; they represent $y_{sa} \in Y_{sa}$, $y_{hip} \in Y_{hip}$, $y_{sk} \in Y_{sk}$, and $y_{nsk} \in Y_{nsk}$. The cost function (42) is used as a measure of quantifying the similarity between the robotic walking and human walking.

The parameters of the desired output functions which result in robotic walking minimising the human-data-based cost are found by solving the constrained optimisation problem:

$$\begin{aligned} &\boldsymbol{\alpha}^* = \arg\min_{\boldsymbol{\alpha} \in \mathbb{R}^{16}} \text{Cost}_{\text{HD}}(\boldsymbol{\alpha}) \\ &\text{s.t.} \quad \boldsymbol{\Delta}(\mathcal{S} \cap \mathbf{Z}_{\boldsymbol{\alpha}}) \subset \mathbf{PZ}_{\boldsymbol{\alpha}} \end{aligned} \tag{43}$$

where the guard, $\mathcal{S}$, is as defined in (26) and $\boldsymbol{\Delta}$ is the reset map given in (27), with $\mathbf{Z}_{\boldsymbol{\alpha}}$ the full zero dynamics surface

$$\begin{aligned} \mathbf{Z}_{\boldsymbol{\alpha}} = \big\{ &(\boldsymbol{\theta}, \dot{\boldsymbol{\theta}}) \in \mathbf{X} : y_1(\boldsymbol{\theta}, \dot{\boldsymbol{\theta}}) = 0, \mathbf{y}_2(\boldsymbol{\theta}) = \mathbf{0}, \\ &L_{\mathbf{f}} \mathbf{y}_2(\boldsymbol{\theta}, \dot{\boldsymbol{\theta}}) = \mathbf{0} \big\} \end{aligned} \tag{44}$$

where all of the desired and actual outputs agree for all time, and $\mathbf{PZ}_{\boldsymbol{\alpha}}$ is the partial zero dynamics surface:

$$\mathbf{PZ}_{\boldsymbol{\alpha}} = \left\{ (\boldsymbol{\theta}, \dot{\boldsymbol{\theta}}) \in \mathbf{X} : \mathbf{y}_2(\boldsymbol{\theta}) = \mathbf{0}, L_{\mathbf{f}} \mathbf{y}_2(\boldsymbol{\theta}, \dot{\boldsymbol{\theta}}) = \mathbf{0} \right\}, \tag{45}$$

where only the RD2 actual and desired outputs agree for all time. The motivation for considering only the RD2 outputs is that it allows the position of the hip or CoM to 'jump' during impact; this compensates for differences between the human and the robotic model being considered.

The optimisation problem in (43) was first considered in (Ames, 2011b) for a subset of the outputs considered in this paper applied to three individual human subjects. In that paper, explicit conditions are given for (43) that provably guarantee stable walking. Moreover, these conditions can be stated only in terms of the parameters, $\boldsymbol{\alpha}$, making them computationally tractable. In particular, the output functions considered (as a result of the fact that they are mutually exclusive) can be used to explicitly solve for a unique point $(\boldsymbol{\theta}(\boldsymbol{\alpha}), \dot{\boldsymbol{\theta}}(\boldsymbol{\alpha})) \in \mathcal{S} \cap \mathbf{Z}_{\boldsymbol{\alpha}}$ such that $\boldsymbol{\Delta}(\boldsymbol{\theta}(\boldsymbol{\alpha}), \dot{\boldsymbol{\theta}}(\boldsymbol{\alpha})) \in \mathbf{PZ}_{\boldsymbol{\alpha}}$. Moreover, the point $(\boldsymbol{\theta}(\boldsymbol{\alpha}), \dot{\boldsymbol{\theta}}(\boldsymbol{\alpha}))$ will, in turn, be the fixed point of a stable periodic orbit, i.e., a stable walking gait. Therefore, using only the human data, through the constrained optimisation problem (43) one automatically obtains a stable walking gait that is as close to 'human-like' as possible.

5 Simulation results

The bipedal model considered in this paper has four degrees of freedom and thus requires four outputs to realise full actuation. The four outputs are obtained by choosing one

element from each output set; in doing so, mutual exclusivity is achieved allowing feedback linearisation to function properly. Many possibilities exist when choosing combinations of outputs but this paper considers six combinations that are of particular interest which are shown in Table 3. The first three combinations utilise hip position to parameterise time while the last three utilise CoM position. This section shows the simulation results of the robotic-model with controllers constructed from each of the six output combinations. The hip-parameterised output combinations are useful due to the simplicity of the parameterisation. The CoM-parameterised output combinations are more computationally-intensive but provide a model which is similar to the SLIP model which has received much attention in the literature (Poulakakis and Grizzle, 2009; Koepl and Hurst, 2011).

5.1 Comparing output combinations

Different output combinations are used to construct the controllers. The parameters of the controllers computed from the optimisation problem (43), together with the optimised costs and correlations, are shown in Table 3. The near-unity correlations imply that the desired outputs of the robot are very close to the human output data. Though all the output combinations make the robotic model walk, the optimised costs indicate a different style of walking for each controller.

Figure 7 illustrates the comparison between the human and robot outputs for each of the six output combinations. For most of the functions shown, the behaviour falls within the range of healthy human walking, with a few outputs showing slight deviations from this range. Thus, the human-inspired control approach results in quantifiably human-like walking.

Table 3 The parameters, correlations, and costs obtained by solving the optimisation problem for each of the 6 output combinations

No.	*Outputs*	$y_1^d = vt,\ y_2^d = e^{-\alpha_4 t}\left(\alpha_1\cos(\alpha_2 t) + \alpha_3\sin(\alpha_2 t)\right) + \alpha_5$							
		v	α_1	α_2	α_3	α_4	α_5	*Cor.*	*Cost*
1	p_{hip}	0.9067	*	*	*	*	*	0.9990	
	θ_{sk}	*	–0.2580	11.7232	0.1500	5.3511	0.3187	0.9716	
	m_{nsl}	*	0.0369	8.3667	0.0813	–3.7162	0.2833	0.9925	
	θ_{nsk}	*	–0.3411	9.8564	0.1326	–0.8382	0.6542	0.9984	1.4683
2	p_{hip}	0.9328	*	*	*	*	*	0.9990	
	ℓ_s	*	0.0128	13.7602	–0.0024	3.5772	0.8196	0.9792	
	m_{nsl}	*	0.0697	7.4236	0.0760	–3.2225	0.2557	0.9941	
	ℓ_{ns}	*	0.0468	10.2764	–0.0086	–0.4053	0.7722	0.9852	0.2348
3	p_{hip}	0.9090	*	*	*	*	*	0.9990	
	ℓ_s	*	0.0144	15.7192	0.0023	6.5409	0.8183	0.9031	
	θ_{vhip}	*	0.0291	–3.6336	–0.0835	–5.4405	–0.6869	0.9983	
	ℓ_{ns}	*	0.0471	10.7483	–0.0017	–0.4654	0.7709	0.9893	0.2829
4	p_{CoM}	0.9268	*	*	*	*	*	0.9993	
	θ_{sk}	*	–0.2697	11.3677	0.1715	5.5976	0.3175	0.9663	
	m_{nsCoM}	*	0.0492	8.2384	0.0956	–3.6704	0.3467	0.9935	
	θ_{nsk}	*	–0.3385	9.7657	0.1436	–0.8578	0.6491	0.9980	1.5172
5	p_{CoM}	0.9387	*	*	*	*	*	0.9993	
	ℓ_{sCoM}	*	0.0140	11.0693	–0.0045	3.4267	0.7088	0.9933	
	m_{nsCoM}	*	0.0385	8.3973	0.0816	–4.1029	0.3537	0.9914	
	ℓ_{nsCoM}	*	0.0463	10.7661	0.0022	–0.3993	0.6643	0.9900	0.2510
6	p_{CoM}	0.9142	*	*	*	*	*	0.9993	
	ℓ_{sCoM}	*	0.0136	11.6954	–0.0041	3.4275	0.7085	0.9893	
	θ_{CoMhip}	*	–0.1265	–4.0895	–0.2344	–2.9362	–0.6414	0.9966	
	ℓ_{nsCoM}	*	0.0435	10.1193	0.0002	–0.5329	0.6662	0.9755	0.3167

Figure 7 Desired output vs. human output over one step for output combinations 1–6, (a) output combination 1, $Y = \{p_{hip}, \theta_{sk}, m_{nsl}, \theta_{nsk}\}$ (b) output combination 2, $Y = \{p_{hip}, \ell_s, m_{nsl}, \ell_{ns}\}$ (c) output combination 3, $Y = \{p_{hip}, \ell_{sk}, \theta_{vhip}, \ell_{nsk}\}$ (d) output combination 4, $Y = \{p_{CoM}, \theta_{sk}, m_{nsCoM}, \theta_{nsk}\}$ (e) output combination 5, $Y = \{p_{CoM}, \ell_{sCoM}, m_{nsCoM}, \ell_{nsCoM}\}$ (f) output combination 6, $Y = \{p_{CoM}, \ell_{sCoM}, \theta_{CoMhip}, \ell_{nsCoM}\}$ (see online version for colours)

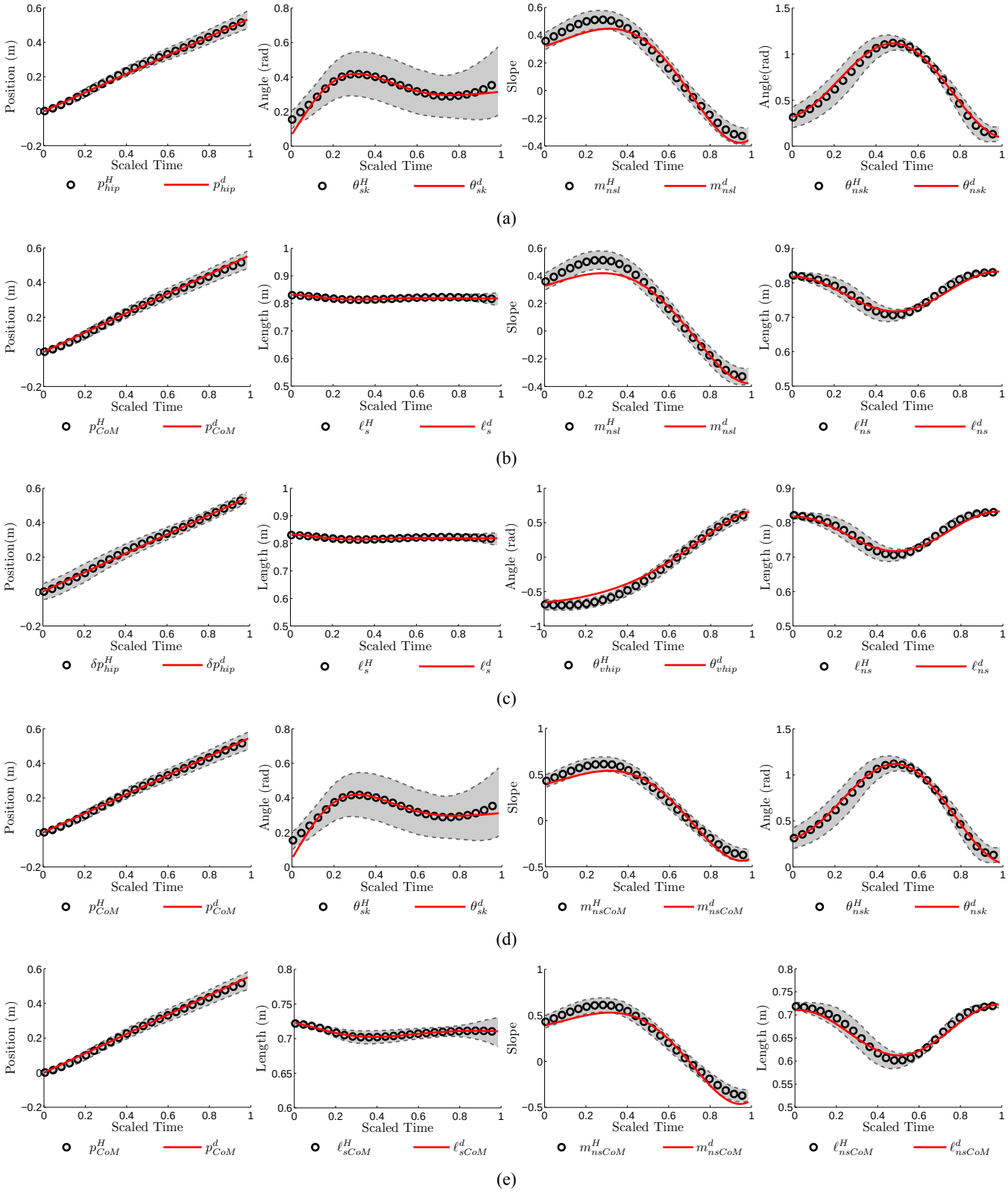

Figure 7 Desired output vs. human output over one step for output combinations 1–6, (a) output combination 1, $Y = \{p_{hip}, \theta_{sk}, m_{nsl}, \theta_{nsk}\}$ (b) output combination 2, $Y = \{p_{hip}, \ell_s, m_{nsl}, \ell_{ns}\}$ (c) output combination 3, $Y = \{p_{hip}, \ell_{sk}, \theta_{vhip}, \ell_{nsk}\}$ (d) output combination 4, $Y = \{p_{CoM}, \theta_{sk}, m_{nsCoM}, \theta_{nsk}\}$ (e) output combination 5, $Y = \{p_{CoM}, \ell_{sCoM}, m_{nsCoM}, \ell_{nsCoM}\}$ (f) output combination 6, $Y = \{p_{CoM}, \ell_{sCoM}, \theta_{CoMhip}, \ell_{nsCoM}\}$ (continued) (see online version for colours)

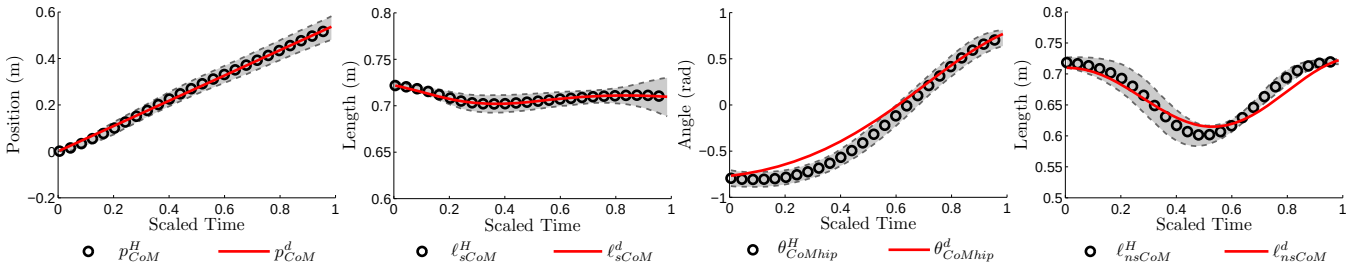

(f)

Figure 8 Simulation results for human model using example output combination 6, (a) the phase portrait shows the existence of a limit cycle and (b) the robot outputs closely mimic the desired human behaviours (see online version for colours)

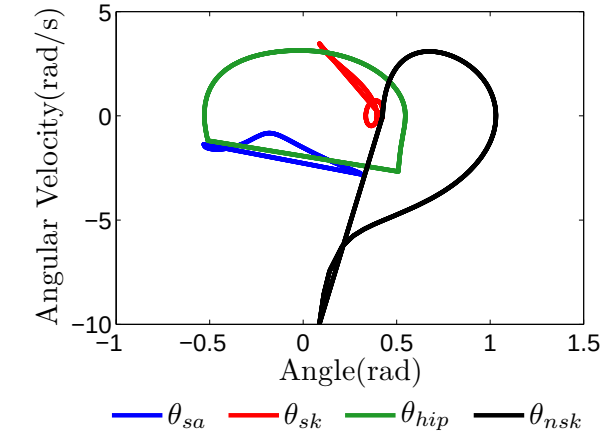

(a)

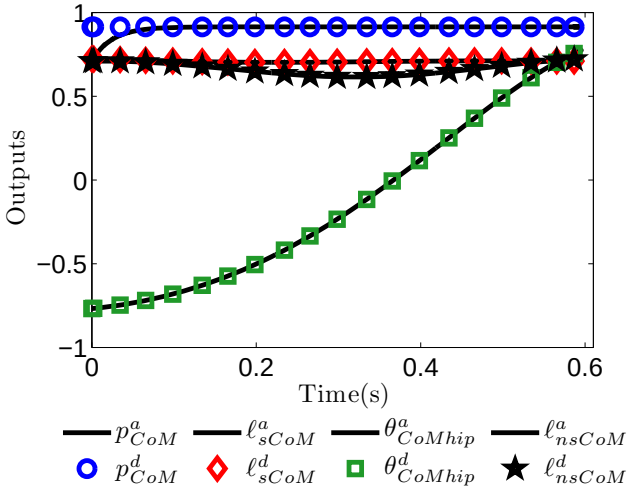

(b)

According to the human-data-based cost, the best output combination is $Y_2 = \{p_{hip}, \ell_s, m_{nsl}, \ell_{ns}\}$, though three of the other combinations have a similarly low cost. Indeed, one can see a trend: the costs are significantly lower for the output combinations which use leg lengths instead of knee angles. For the sake of clarity, output combination 6, $Y_6 = \{p_{CoM}, \ell_{sCoM}, \theta_{CoMhip}, \ell_{nsCoM}\}$, is used as an example since it represents the human and robot as a compass-gait biped based upon the position of the CoM. The simulated walking gait is shown in Figure 9(b) [which can be compared against a human walking gait plotted from the experimental data in Figure 9(a)]. This walking gait was achieved by using control gain $\varepsilon = 20$ in (38) and the parameters, α, of the desired output in Table 3. Figure 8 shows the phase portraits from the simulation. These phase portraits clearly show a closed periodic orbit or limit cycle. In other words, the phase portraits indicate the existence of a walking gait. Stability is examined using the well-known technique of Poincaré analysis (Morris and Grizzle, 2005; Parker and Chua, 1989; Wendel and Ames, 2010). Specifically, the Poincaré section is chosen to be the guard. Then a linearisation of the Poincaré map about a fixed point provides a means for determining stability. Specifically, the Poincaré map is a discrete map, so stability exists when the eigenvalues of the linearisation of this map have magnitudes below unity. One can see from the magnitudes of the eigenvalues in Figure 10 that all simulations show exponentially stable periodic orbits or, in other words, exhibit stable steady state walking.

5.2 *Outputs and joint angles*

For output combination 6, Y_6, Figure 8 shows the actual outputs, y_i^a, and the desired outputs, y_i^d, over one step. One can see that the RD2 outputs, y_{sk}, y_{hip}, and y_{nsk}, match up to the extent observable through Figure 8. One can also see that the RD1 output, y_{sa}, starts off the HZD surface, and indeed this occurs by design as a ramification of PHZD. Foot-strike drives this output away from the HZD surface as no constraint is imposed on the optimisation which would prevent this. Yet, using the theory presented and previous work (Ames, 2011b), provably stable walking gaits can be found which leverage the concepts of PHZD.

Figure 9 Comparison of human walking and robotic walking for example output combination 6, (a) human gait plotted from experimental data (b) robotic (MH) model simulation gait (c) AMBER simulation gait (see online version for colours)

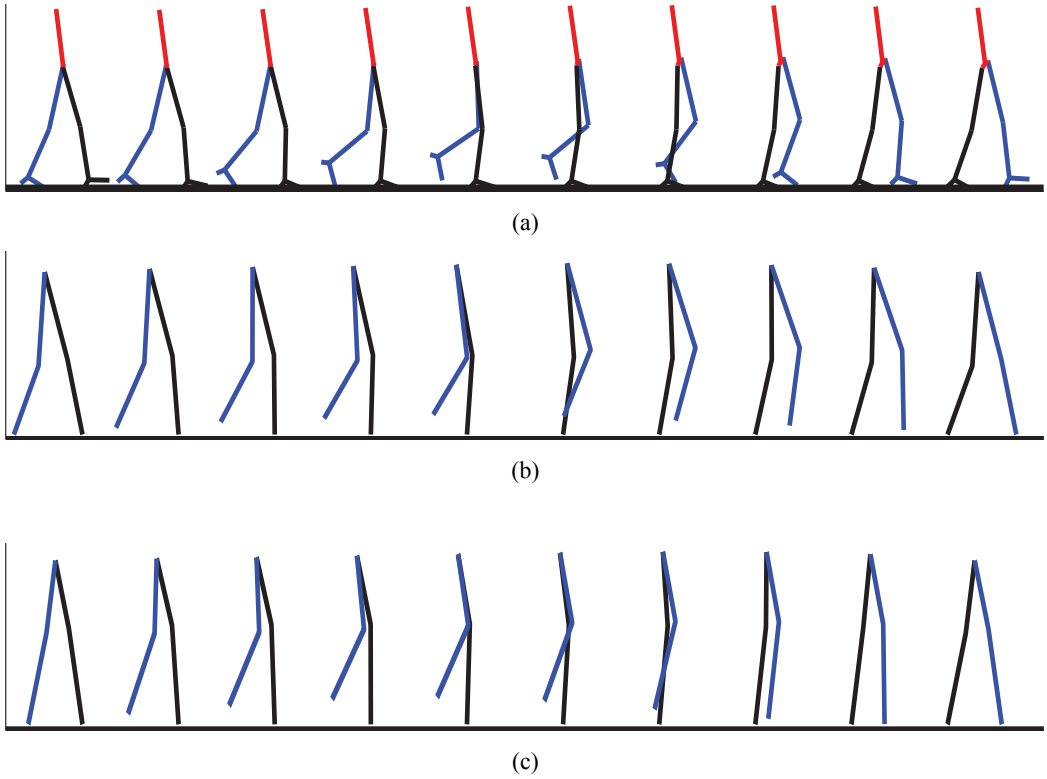

Figure 10 Eigenvalues from simulation of human models H1–6 and AMBER model A6 (see online version for colours)

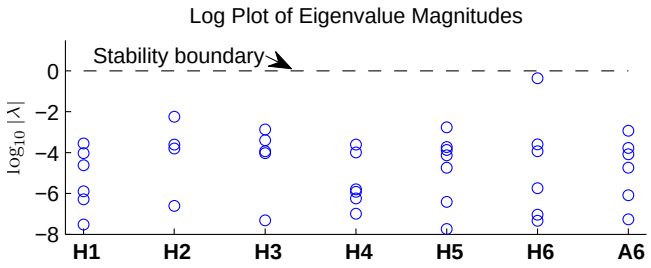

Figure 11 shows the evolution of the configuration variables, $\boldsymbol{\theta}$, throughout the walking gait, for example, output combination 6. For this output combination, none of the angles of the system are directly controlled so as to agree with the human angle data (since only the outputs, which are functions of the angles, are required to match). Despite this, the angles still match up quite well with normal human walking. Consequently, the walking gait is relatively humanlike and, in fact, this conclusion is further substantiated by visual comparison between the human gait in Figure 9(a) and the robot models in Figure 9(b) and Figure 9(c). For an even better comparison, the reader is encouraged to watch videos of the various gaits online (Video: Robotic Walking, 2011).

6 Applications to physical robots

In order to strengthen the results presented, human-inspired control design is applied to the robot AMBER (Ames, 2011a) to show that the prescribed modelling approach is practical and useful on robots that may not be human-like in design. This robot (see Figure 6) has five links: two calves, two thighs, and a hip. AMBER was modelled in SolidWorks which provided a straightforward method for obtaining physical parameters including lengths, masses, and inertias. Some of the physical parameters are given in Table 4; these parameters are analogous to the MH model. For the sake of brevity some of the physical parameters such as inertias are omitted. The importance of this robot is that it differs from the MH model in that:

1 the mass and length distribution is no longer 'human-like'

2 it models a real physical biped.

Note that technically this robot has an additional torso angle as a result of the hip; this angle was incorporated into the optimisation through the procedures outlined in this paper; the specifics will not be discussed as this work intends to focus on lower limb ambulation. For more details, see Ames (2012).

Recall that the MH model has only four links as no hip is present. A comparison between this model and AMBER can be more easily drawn if a four-link version of AMBER is considered. To this end, a simulation model was constructed which consisted of only the calves and thighs. Then, the procedures in the previous sections were applied to the AMBER model and the six output combinations were tested. Due to space constraints, the results from only one simulation are shown; for comparison's sake, the example simulation is the same as that shown for the human: output combination 6. The optimisation parameters are shown in Table 5. The corresponding output functions are shown in Figure 12 and, remarkably, the walking functions still lie within the range of healthy human walking even though AMBER is less humanlike in design than the MH model. In analogy to Figure 11, the configuration variables, $\boldsymbol{\theta}$, for example, output combination 6 is plotted in Figure 13. These plots show some deviation from healthy human walking. This occurs mostly near the end as a result of requiring hybrid zero dynamics which essentially sets the angular velocities at the beginning and end of a step to match up. In spite of this shortcoming, the walking produced is still quite human-like with respect to the outputs, and the walking tiles in Figure 9(c) are similar to the human and MH model tiles in Figure 9(a) and Figure 9(b), respectively. Finally, for the simulated gait, the phase portraits are shown in Figure 14(a) and the outputs are shown in Figure 14(b). From the outputs, one can see that PHZD has indeed been realised. For a movie of the walking obtained through these general principles [as outlined in Ames (2012)], see the video at Video: AMBER Walking (2011).

Table 4 The physical parameters used to model AMBER

m_h (kg)	m_t (kg)	m_c (kg)	L_t (cm)	L_c (cm)	r_t (cm)	r_c (cm)
8.04	6.06	2.14	26.11	34.80	12.82	28.24

Table 5 Parameters for output combination 6 optimised for AMBER

No.	*Outputs*	$y_1^d = vt,\ y_2^d = e^{-\alpha_4 t}\left(\alpha_1\cos(\alpha_2 t) + \alpha_3\sin(\alpha_2 t)\right) + \alpha_5$							
		v	α_1	α_2	α_3	α_4	α_5	*Cor.*	*Cost*
6	p_{CoM}	0.7193	*	*	*	*	*	0.9887	
	ℓ_{sCoM}	*	0.0053	8.2524	–0.0306	1.0482	0.4897	0.9975	
	θ_{CoMhip}	*	–0.0699	4.7295	0.0901	–4.8442	–0.8045	0.9683	
	ℓ_{nsCoM}	*	0.0360	10.4153	0.0048	0.2581	0.4684	0.9844	0.4583

Figure 11 Angles computed from human data over one step and the corresponding angles of the robotic model (see online version for colours)

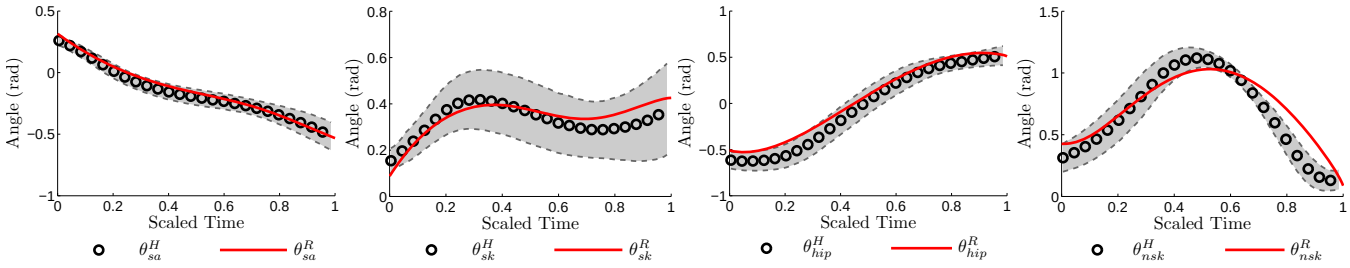

Notes: The superscript *H* represents the MH angles with the error bands showing the one standard deviation. The superscript *R* represents the angles of the robot.

Figure 12 Desired output vs. actual output over one step for output combination 6 for AMBER (see online version for colours)

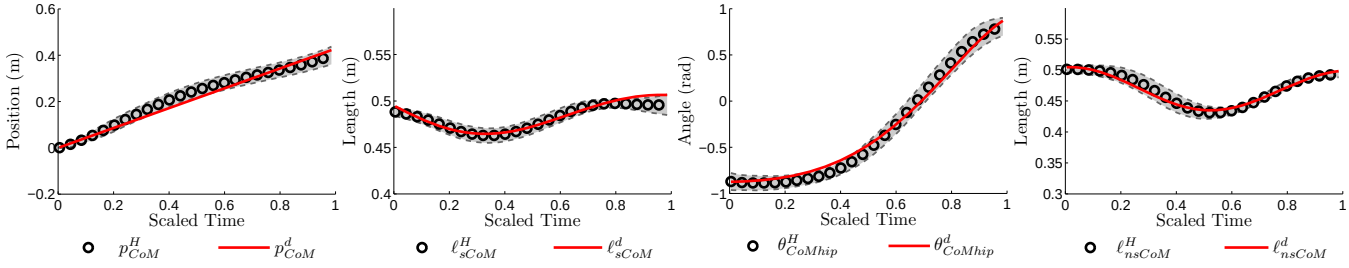

Figure 13 The configuration variables (angles) for healthy human walking and for AMBER, for example, output combination 6 (see online version for colours)

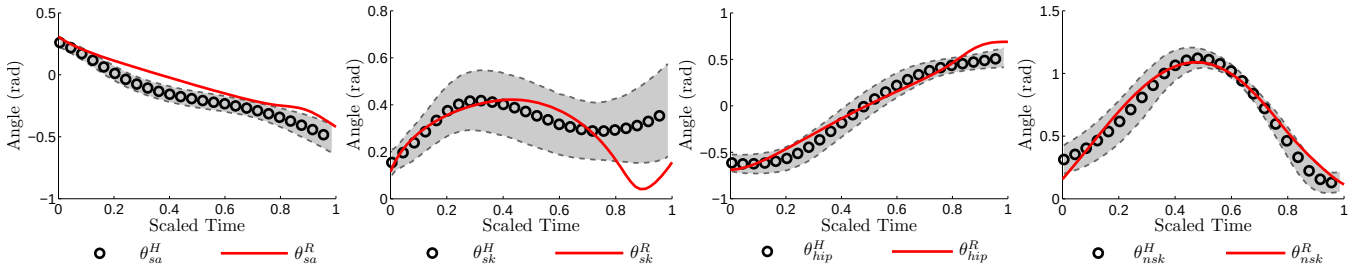

Figure 14 Simulation results for AMBER using example output combination 6. As in Figure 8, (a) the phase portrait shows the existence of a limit cycle and (b) AMBER's outputs closely mimic the desired human behaviours (see online version for colours)

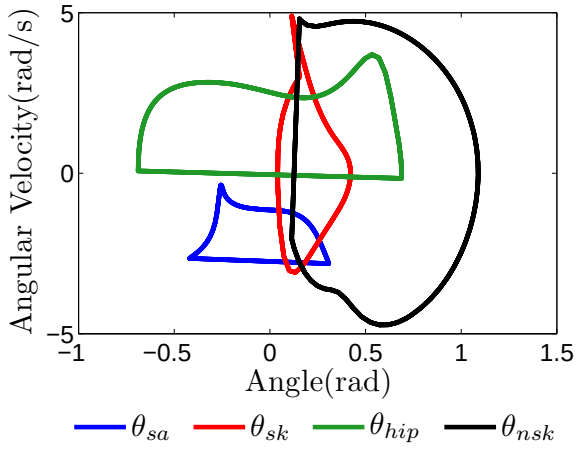

(a)

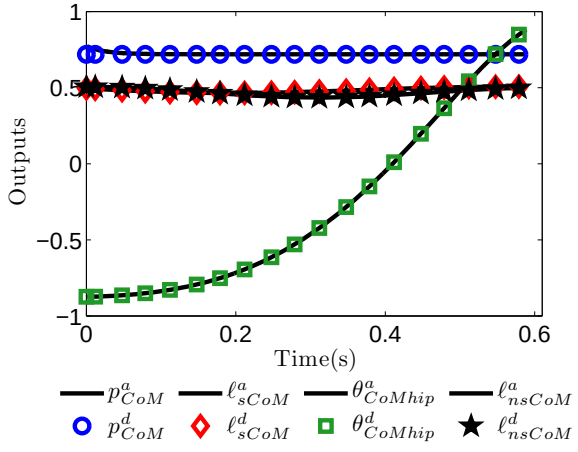

(b)

7 Conclusions

This paper presented a human-inspired framework for achieving human-like bipedal locomotion on robotic models. Unlike other biomechanics work in which complex neuromuscular or internal force models are considered, the human-inspired method provides a simple 'black box' model of human walking with the inputs being control and the outputs being functions on the kinematics of a model. Examination of various kinematics outputs on human behaviour indicated that a class of simple mathematical functions – namely, canonical walking functions – can be used to faithfully represent specific behaviours of human walking over the course of a step such as the angle of a knee or the slope of a leg. The possible outputs, in this paper O1-12, were divided up into mutually exclusive sets. For the purposes of control design, one function was chosen from each set and the optimisation proceeded from there. Five parameters comprise a canonical walking function, and, through optimisation, these parameters can be chosen to provide the best possible fit to experimental human kinematics data. When directly fit to the data without any constraints imposed, the correlations for the functions examined in this study were found to be over 0.9 for all functions and even very close to unity for many of them. This statistical measure indicates that the functions do a very impressive job of representing the fitted data.

These functions were modified using a state-based parameterisation for time which resulted in autonomous functions. When these functions are tracked using feedback linearisation, a zero dynamics surface can be established but impacts introduce challenges by throwing the system off this surface. This was dealt with by defining the concept of a partial hybrid zero dynamics and imposing constraints on the parameter optimisation to ensure that PHZD was achieved. In the end, the human-inspired framework is capable of taking experimental data and a robotic model and producing a control law which results in a provably exponentially stable periodic orbit or stable walking. This was demonstrated in various simulations in which different, mutually-exclusive walking functions were chosen and the results were stable human-like walking for a MH model studied in this paper as well as for the robot AMBER.

Figure 15 Stable walking gait of biped AMBER (see online version for colours)

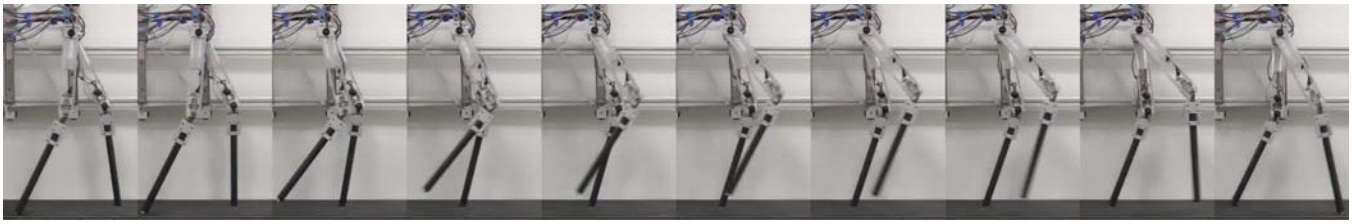

Source: This was achieved in Yadukumar et al. (2012)

Future work will be aimed at extending the results achieved for lower-limb 2D walking to three dimensions. In particular, output functions satisfying (OC1-3), as outlined in Section 1, must be found for the coronal dynamics of a human. As in the 2D case presented here, these functions must not only satisfy properties that allow them to be utilised for robotic control, but must also lead to insight into the underlying mechanisms of human walking. Studying the behaviour of the upper limbs during locomotion could also be fruitful, especially if this behaviour can also be characterised by the canonical walking functions presented here. This would imply that the entire human system essentially consists of linear mass-spring-damper systems when ambulating. Finally, the outputs considered in this work were kinematic in nature. The motivation for considering kinematic outputs was that the dynamics of humans and robots can differ greatly. An interesting research question is whether the kinematic constraints that were discovered can lead to a greater understanding of the dynamics internal to humans when walking. Combining the MH model considered in this paper with models for musculature forcing would potentially provide interesting insights in this direction. Results of this form could yield an important understanding of human locomotion that could be applied to both bipedal robotics and areas in which humans and robots interact such as prosthetics.

Finally, as the ultimate goal of this work is to provide a framework for obtaining human-like bipedal robotic walking, it is necessary to ultimately realise these ideas on physical bipedal robots. To this end, the authors have already implemented these ideas on AMBER (as discussed in this paper) and NAO (a commercially available 3D bipedal robot). While the technical details related to implementation are not within the scope of this paper, it is important to note that for both robotic platforms human-inspired robotic walking was obtained (Ames, 2012; Ames et al., 2012). In particular, gait tiles of the result walking gait for AMBER can be seen in Figure 15 and a video of the walking gait can be found at Video: AMBER Walking (2011). While these implementation results are only the first step towards obtaining human-like robotic walking, the results presented in this paper have the potential to further bridge the gap between human and robotic walking. The consequences of understanding the underlying mechanisms related to walking could be far-reaching, yielding robots able to achieve the versatility of motion that humans display with ease.

References

Ambrose, R., Aldridge, H., Askew, R., Burridge, R., Bluethmann, W., Diftler, M., Lovchik, C., Magruder, D. and Rehnmark, F. (2000) 'Robonaut: NASA's space humanoid', *IEEE Intelligent Systems*, Vol. 15, No. 4, pp.57–63.

Ames, A.D. (2011a) 'AMBER Lab – home', available at http://www.bipedalrobotics.com (accessed on 09/01/12).

Ames, A.D. (2011b) 'First steps toward automatically generating bipedal robotic walking from human data', in *8th Intl. Workshop on Robot Motion and Control*, Gronów.

Ames, A.D. (2012) 'First steps toward underactuated human-inspired bipedal robotic walking', in *IEEE Intl. Conf. on Robotics and Automation. Submitted*, available upon request.

Ames, A.D., Cousineau, E.A. and Powell, M.J. (2012) 'Dynamically stable robotic walking with NAO via human-inspired hybrid zero dynamics', in *15th Intl. Conf. on Hybrid Systems: Computation and Control*, Beijing.

Ames, A.D., Gregg, R.D. and Spong, M.W. (2007) 'A geometric approach to three-dimensional hipped bipedal robotic walking', in *45th Conference on Decision and Control*, San Diago, CA.

Ames, A.D., Sinnet, R.W. and Wendel, E.D.B. (2009) 'Three-dimensional kneed bipedal walking: a hybrid geometric approach', in Majumdar, R. and Tabuada, P. (Eds.): *12th ACM Intl. Conf. on Hybrid Systems: Computation and Control, Lecture Notes in Computer Science – HSCC 2009*, Vol. 5469, pp.16–30, Springer, San Francisco.

Ames, A.D., Vasudevan, R. and Bajcsy, R. (2011) 'Human-data based cost of bipedal robotic walking', in *Hybrid Systems: Computation and Control*, pp.151–60, Chicago.

Anderson, F.C. and Pandy, M.G. (2001) 'Dynamic optimization of human walking', *ASME J. of Biomech. Eng.*, Vol. 123, No. 5, pp.381–90.

Au, S.K. and Herr, H. (2008) 'Powered ankle-foot prosthesis', *IEEE Robotics & Automation Magazine*, Vol. 15, No. 3, pp.52–59.

Au, S.K., Dilworth, P. and Herr, H. (2006) 'An ankle-foot emulation system for the study of human walking biomechanics', in *IEEE Intl. Conf. on Robotics and Automation*, pp.2939–2945, Orlando.

Bellmann, M., Schmalz, T. and Blumentritt, S. (2010) 'Comparative biomechanical analysis of current microprocessor-controlled prosthetic knee joints', *Archives of Physical Medicine and Rehabilitation*, Vol. 91, No. 4, pp.644–652.

Bergmann, G., Graichen, F. and Rohlmann, A. (1993) 'Hip joint loading during walking and running, measured in two patients', *J. of Biomech.*, Vol. 26, No. 8, pp.969–990.

Bojanic, D.M., Petrovacki-Balj, B.D., Jorgovanovic, N.D. and Ilic, V.R. (2011) 'Quantification of dynamic EMG patterns during gait in children with cerebral palsy', *J. of Neuroscience Methods*, Vol. 198, No. 2, pp.325–331.

Brubaker, M.a. and Fleet, D.J. (2008) 'The kneed walker for human pose tracking', *IEEE Conf. on Computer Vision and Pattern Recognition*, pp.1–8.

Cifrek, M., Medved, V., Tonković, S. and Ostojić, S. (2009) 'Surface EMG based muscle fatigue evaluation in biomechanics', *Clinical Biomech.*, Vol. 24, No. 4, pp.327–340.

Deluzio, K. (1997) 'Principal component models of knee kinematics and kinetics: normal vs. pathological gait patterns', *Human Movement Science*, Vol. 16, Nos. 2–3, pp.201–217.

Espiau, B. and Goswami, A. (1994) 'Compass gait revisited', in *IFAC Symposium on Robot Control*, pp.839–846, Capri.

Glaister, B., Schoen, J., Orendurff, M. and Klute, G. (2009) 'A mechanical model of the human ankle in the transverse plane during straight walking: Implications for prosthetic design', *J. of Biomech. Eng.*, Vol. 131, No. 3, p.034501.

Glitsch, U. and Baumann, W. (1997) 'The three-dimensional determination of internal loads in the lower extremity', *ASME J. of Biomech. Eng.*, Vol. 30, No. 11, pp.1123–1131.

Goswami, A., Thuilot, B. and Espiau, B. (1998) 'A study of the passive gait of a compass-like biped robot: symmetry and chaos', *Intl. J. of Robotics Research*, Vol. 17, No. 12, pp.1282–301.

Grimes, D., Flowers, W. and Donath, M. (1977) 'Feasibility of an active control scheme for above knee prostheses', *J. of Biomech. Eng.*, Vol. 99, No. 77, p.215.

Grizzle, J.W., Chevallereau, C., Ames, A.D. and Sinnet, R.W. (2010) '3D bipedal robotic walking: models, feedback control, and open problems', in *IFAC Symposium on Nonlinear Control Systems*, Bologna.

Heller, M.O., Bergmann, G., Deuretzbacher, G., Dürselen, L., Pohl, M., Claes, L., Haas, N.P. and Duda, G.N. (2001) 'Musculoskeletal loading conditions at the hip during walking and stair climbing', *J. of Biomech.*, Vol. 34, No. 1, pp.883–893.

Herr, H. and Wilkenfeld, A. (2003) 'User-adaptive control of a magnetorheological prosthetic knee', *Industrial Robot: An Intl. J.*, Vol. 30, No. 1, pp.42–55.

Holmes, P., Full, R.J., Koditschek, D. and Guckenheimer, J. (2006) 'The dynamics of legged locomotion: models, analyses, and challenges', *SIAM Review*, Vol. 48, No. 2, pp.207–304.

Hürmüzlü, Y. and Marghitu, D.B. (1994) 'Rigid body collions of planar kinematic chains with multiple contact points', *Intl. J. of Robotics Research*, Vol. 13, No. 1, pp.82–92.

Joshi, D. and Anand, S. (2010) 'Study of circular cross correlation and phase lag to estimate knee angle: an application to prosthesis', *Intl. J. of Biomechatronics and Biomedical Robotics*, Vol. 1, No. 2, pp.99–103.

Ko, S.U., Ling, S.M., Winters, J. and Ferrucci, L. (2009) 'Age-related mechanical work expenditure during normal walking: the Baltimore longitudinal study of aging', *J. of Biomech.*, Vol. 42, No. 12, pp.1834–1839.

Koepl, D. and Hurst, J.W. (2011) 'Force control for planar spring-mass running', in *IEEE International Conference on Intelligent Robots and Systems (IROS)*.

Kramer, P.A. (2010) 'The effect on energy expenditure of walking on gradients or carrying burdens', *American J. of Human Biol.: The Official J. of the Human Biol. Council*, Vol. 22, No. 4, pp.497–507.

Kumar, N., Kunju, N., Kumar, A. and Sohi, B. (2010) 'Knowledge base generation and its implementation for control of above knee prosthetic device based on SEMG and knee flexion angle', *Intl. J. of Biomechatronics and Biomedical Robotics*, Vol. 1, No. 2, p.126.

Kuo, A.D. (2002) 'Energetics of actively powered locomotion using the simplest walking model', *J. of Biomech. Eng.*, Vol. 124, No. 1, pp.113–120.

Kuo, A.D. (2007) 'The six determinants of gait and the inverted pendulum analogy: a dynamic walking perspective', *Human Movement Science*, Vol. 26, No. 4, pp.617–656.

Martinez-Villalpando, E.C., Weber, J., Elliott, G. and Herr, H. (2008) 'Design of an agonist-antagonist active knee prosthesis', *2nd IEEE RAS & EMBS Intl. Conf. on Biomedical Robotics and Biomechatronics*, pp.529–534.

McGeer, T. (1990) 'Passive dynamic walking', *Intl. J. of Robotics Research*, Vol. 9, No. 2, pp.62–82.

Morgenroth, D.C., Segal, A.D., Zelik, K.E., Czerniecki, J.M., Klute, G.K., Adamczyk, P.G., Orendurff, M.S., Hahn, M.E., Collins, S.H. and Kuo, A.D. (2011) 'The effect of prosthetic foot push-off on mechanical loading associated with knee osteoarthritis in lower extremity amputees', *Gait & Posture*, October, Vol. 34, No. 4, pp.502–507, Elsevier.

Morris, B. and Grizzle, J.W. (2005) 'A restricted Poincaré map for determining exponentially stable periodic orbits in systems with impulse effects: application to bipedal robots', in *44th IEEE Conf. on Decision and Control and European Control Conf.*, Sevilla.

Neptune, R.R., Kautz, S.A. and Zajac, F.E. (2001) 'Contributions of the individual ankle plantar flexors to support, forward progression and swing initiation during walking', *J. of Biomech.*, Vol. 34, No. 11, pp.1387–1398.

Nyan, M.N., Tay, F.E.H. and Mah, M.Z.E. (2008) 'Application of motion analysis system in pre-impact fall detection', *J. of Biomech.*, Vol. 41, No. 10, pp.2297–2304.

Ogura, Y., Shimomura, K., Kondo, A., Morishima, A., Okubo, T., Momoki, S., Lim, H. and Takanishi, A. (2006) 'Human-like walking with knee stretched, heel-contact and toe-off motion by a humanoid robot', in *IEEE/RSJ Intl. Conf. on Intelligent Robots and Systems*, pp.3976–3981.

Olenšek, A. and Matjačić, Z. (2007) 'Human-like control strategy of a bipedal walking model', *Robotica*, Vol. 26, No. 3, pp.295–306.

Pandy, M.G. and Berme, N. (1988) 'A numerical method for simulating the dynamics of human walking', *J. of Biomech.*, Vol. 21, No. 12, pp.1043–1051.

Parker, T.S. and Chua, L.O. (1989). *Practical Numerical Algorithms for Chaotic Systems*, Springer, New York.

Perry, J. and Burnfield, J. (2010) *Gait Analysis: Normal and Pathological Function*, 2nd ed., Slack Incorporated, Thorofare.

Popović, D., OÄ§uztöreli, M.N. and Stein, R.B. (1991) 'Optimal control for the active above-knee prosthesis', *Annals of Biomedical Eng.*, Vol. 19, No. 2, pp.131–150.

Popovic, M., Hofmann, A. and Herr, H. (2004) 'Angular momentum regulation during human walking: biomechanics and control', in *IEEE Intl. Conf. on Robotics and Automation*, April, Vol. 3, pp.2405–2411, New Orleans.

Poulakakis, I. and Grizzle, J.W. (2009) 'The spring loaded inverted pendulum as the hybrid zero dynamics of an asymmetric hopper', *IEEE Trans. on Automatic Control*, Vol. 54, No. 8, pp.1779–1793.

Rand, D., Eng, J.J., Tang, P-F., Jeng, J-S., and Hung, C. (2009) 'How active are people with stroke?: use of accelerometers to assess physical activity', *Stroke; A J. of Cerebral Circulation*, Vol. 40, No. 1, pp.163–168.

Rodgers, M.M. (1988) 'Dynamic biomechanics of the normal foot and ankle during walking and running', *Physical Therapy*, Vol. 68, No. 12, pp.1822–1830.

Sastry, S.S. (1999) *Nonlinear Systems: Analysis, Stability and Control*, Springer, New York.

Scarfogliero, U. and Folgheraiter, M. (2004) 'Advanced steps in biped robotics: innovative design and intuitive control through spring-damper actuator', *4th IEEE/RAS Intl. Conf. on Humanoid Robots*, November, pp.196–214, Los Angeles.

Schaub, T., Scheint, M., Sobotka, M., Seiberl, W. and Buss, M. (2009) 'Effects of compliant ankles on bipedal locomotion', in *EEE/RSJ Intl. Conf. on Intelligent Robots and Systems*.

Scott, S.H. and Winter, D.A. (1993) 'Biomechanical model of the human foot: kinematics and kinetics during the stance phase of walking', *J. of Biomech*., Vol. 26, No. 9, pp.1091–1104.

Seireg, A. and Arvikar, R.J. (1975) 'The prediction of muscular load sharing and joint forces in the lower extremities during walking', *J. of Biomech*., March, Vol. 8, No. 2, pp.89–102.

Shamaei, K. and Dollar, A.M. (2011) 'On the mechanics of the knee during the stance phase of the gait', in *IEEE Intl. Conf. on Rehabilitation Robotics (ICORR)*, Zurich, Switzerland.

Siegler, S. and Liu, W. (1997) *Three-Dimensional Analysis of Human Locomotion*, Chapter Inverse Dynamics in Human Locomotion, pp.191–209, John Wiley & Sons, New York.

Sinnet, R.W. and Ames, A.D. (2009) '2D bipedal walking with knees and feet: a hybrid control approach', in *Joint 48th IEEE Conf. on Decision and Control and 28th Chinese Control Conf*., pp.3200–3207, Shanghai.

Sinnet, R.W. and Ames, A.D. (2012) 'Bio-inspired feedback control of three-dimensional humanlike bipedal robots', *J. of Robotics and Mechatronics*, Vol. 24, No. 4, pp.595–601.

Sinnet, R.W., Powell, M.J., Shah, R.P. and Ames, A.D. (2011) 'A human-inspired hybrid control approach to bipedal robotic walking', in *18th IFAC World Congress*, Milan.

Spong, M.W. and Bullo, F. (2005) 'Controlled symmetries and passive walking', *IEEE Trans. on Automatic Control*, Vol. 50, No. 7, p.1025–1031.

Srinivasan, S., Raptis, I.A. and Westervelt, E.R. (2008) 'Low-dimensional sagittal plane model of normal human walking', *ASME J. of Biomech. Eng*., October, Vol. 130, No. 5.

Srinivasan, S., Westervelt, E. and Hansen, A. (2009) 'A low-dimensional sagittal-plane forward-dynamic model for asymmetric gait and its application to study the gait of transtibial prosthesis users', *ASME J. of Biomech. Eng*., March, Vol. 131, No. 3, p.031003.

Torrealba, R., Fernández-López, G. and Grieco, J. (2008) 'Towards the development of knee prostheses: review of current researches', *Kybernetes*, Vol. 37, Nos. 9/10, pp.1561–1576.

Video: AMBER Walking (2011) 'AMBER walking with human-inspired control', available at http://www.youtube.com/watch?v=vB3MF1q3wHA (accessed on 09/01/2012).

Video: Robotic Walking (2011) 'Video of the robotic walking obtained for all 6 output combinations', available at http://www.youtube.com/watch?v=SYXWoNU8QUE (accessed on 09/01/2012).

Watt, J.R., Franz, J.R., Jackson, K., Dicharry, J., Riley, P.O. and Kerrigan, D.C. (2010) 'A three-dimensional kinematic and kinetic comparison of overground and treadmill walking in healthy elderly subjects', *Clinical Biomech*., Vol. 25, No. 5, pp.444–449.

Wendel, E.D.B. and Ames, A.D. (2010) 'Rank properties of Poincaré maps for hybrid systems with applications to bipedal walking', in *Hybrid Systems: Computation and Control*, pp.151–160, Stockholm.

Westervelt, E.R., Grizzle, J.W. and Koditschek, D.E. (2003) 'Hybrid zero dynamics of planar biped walkers', *IEEE Trans. on Automatic Control*, Vol. 48, No. 1, pp.42–56.

Westervelt, E.R., Grizzle, J.W., Chevallereau, C., Choi, J.H. and Morris, B. (2007) *Feedback Control of Dynamic Bipedal Robot Locomotion*, CRC Press, Boca Raton.

Winter, D.A. (1990) *Biomechanics and Motor Control of Human Movement*, 2nd ed., Wiley-Interscience, New York.

Wong, A.Y.C., Sangeux, M. and Baker, R. (2010) 'Calculation of joint moments following foot contact across two force plates', *Gait & Posture*, Vol. 31, No. 2, pp.292–293.

Yadukumar, S.N., Pasupuleti, M. and Ames, A.D. (2012) 'From formal methods to algorithmic implementation of human inspired control on bipedal robots', in *10th Intl. Work. on the Algorithmic Foundations of Robotics (WAFR)*, Springer, Boston.

Zampeli, F., Moraiti, C.O., Xergia, S., Tsiaras, V.a., Stergiou, N. and Georgoulis, A.D. (2010) 'Stride-to-stride variability is altered during backward walking in anterior cruciate ligament deficient patients', *Clinical Biomech*., Vol. 25, No. 10, pp.1037–1041.